A refinement of the processes controlling dissolved copper and nickel biogeochemistry: insights from the pan-Arctic

Laramie T. Jensen[1,2] Jay T. Cullen[3], Sarah L. Jackson[3,4], Loes J.A. Gerringa[5], Dorothea Bauch[6], Rob Middag[5], Robert M. Sherrell[7], Jessica N. Fitzsimmons[1]

[1]Department of Oceanography, Texas A&M University, College Station, TX, USA

[2] Cooperative Institute for Climate, Ocean, and Ecosystem Studies, University of Washington, Seattle, WA, USA

[3]School of Earth and Ocean Sciences, University of Victoria, Victoria, BC V8P 5C2, Canada

[4]Research School of Earth Sciences, The Australian National University, Canberra, ACT 0200, Australia

[5]Royal Netherlands Institute for Sea Research (NIOZ), Department of Ocean Systems, Texel, the Netherlands

[6]Leibniz Laboratory for Radiometric Dating and Stable Isotope Research, Kiel University, Kiel, Germany and GEOMAR Helmholtz Centre for Ocean Research, Kiel, Germany

[7] Department of Marine and Coastal Sciences and Department of Earth and Planetary Sciences, Rutgers University, New Brunswick, NJ, USA

Key points:

- Dissolved Cu and Ni are linearly correlated in the Arctic Ocean
- Cu is sourced primarily from rivers, while Ni is also sourced from sediments on the Chukchi Shelf
- Cu and Ni are attenuated within the Canadian Arctic Archipelago along transit towards Baffin Bay
- Concentrations of both Cu and Ni are lower in Western than in Eastern Arctic deep waters
- Vertical biological signals are absent for Cu and Ni in central Arctic waters

Abstract

Recent studies, including many from the GEOTRACES program, have expanded our knowledge of trace metals in the Arctic Ocean, an isolated ocean dominated by continental shelf and riverine inputs. Here we report a unique, pan-Arctic linear relationship between dissolved copper (Cu) and nickel (Ni) present north of 60°N that is absent in other oceans. The correlation is driven primarily by high Cu and Ni concentrations in the low salinity, river-influenced surface Arctic and low, homogeneous concentrations in Arctic deep waters, opposing their typical global distributions. Rivers are a major source of both metals, which is most evident within the central Arctic's Transpolar Drift. Local decoupling of the linear Cu-Ni relationship along the Chukchi Shelf and within the Canada Basin upper halocline reveals that Ni is additionally modified by biological cycling and shelf sediment processes, while Cu is mostly sourced from riverine inputs and influenced by mixing. This observation highlights differences in their chemistries: Cu is more prone to complexation with organic ligands, stabilizing its riverine source fluxes into the Arctic, while Ni is more labile and is dominated by biological processes. Within the Canadian Arctic Archipelago, an important source of Arctic water to the Atlantic Ocean, contributions of Cu and Ni from meteoric waters and the halocline are attenuated during transit to the Atlantic. Additionally, Cu and Ni in deep waters diminish with age due to isolation from surface sources, with higher concentrations in the younger Eastern Arctic basins and lower concentrations in the older Western Arctic basins.

Introduction

Trace metals serve as essential micronutrients for marine phytoplankton as well as tracers of important biogeochemical processes. Nickel (Ni) is classified as a "nutrient-type" element based on its macronutrient-like profile shape. Nutrient-type elemental cycling is relatively simple compared to copper (Cu), for example, which is a "hybrid-type" element because it often has a distinct, linearly-increasing concentration trend with depth, indicating that abiotic processes also play a role in controlling its distribution, in conjunction with biological cycling [Bruland et al., 2014]. Copper serves as an essential metalloenzyme center for proteins such as cytochrome oxidase [Wood, 1978], iron acquisition proteins [Maldonado et al., 2006], and denitrification proteins [Granger and Ward, 2003], and at low oceanic Cu concentrations, Cu even has the potential to co-limit primary production alongside other micronutrients [Annett et al., 2008]. However, high concentrations of available Cu are toxic to phytoplankton [Moffett et al., 1997], which can be mitigated by surface complexation of Cu by organic ligands (>95%, [Coale and Bruland, 1988; Moffett and Brand, 1996]) that buffer labile Cu concentrations at non-toxic levels more conducive to phytoplankton growth [Bruland et al., 2014].

Scavenging onto particles facilitates Cu removal from deep waters [Boyle et al., 1977; Moore, 1978; Noriki et al., 1998], explaining why its concentration does not increase as much as the nutrient-type metals along the deep water flow path of thermohaline circulation. However, copper's profile increases linearly with depth, suggesting a sediment/deep water source [Hines et al., 1984; Biller and Bruland, 2013] or possible reversible scavenging at depth, similar to thorium [Bacon and Anderson, 1982]. Margin and benthic sources have been proposed as significant inputs of Cu to both surface and bottom waters [Boyle et al., 1981; Heggie et al., 1987], pointing

45 to the important role of sediments alongside rivers and aerosol fluxes, which are the major
46 external sources of Cu to the global ocean [Richon and Tagliabue, 2019].
47 Nickel also serves as an essential micronutrient and has a “macronutrient-like” profile
48 shape with surface depletion and regeneration at depth, although it is not fully depleted at the
49 surface [Schlitzer et al., 2018; Middag et al., 2020]. As a protein metal center, it catalyzes the
50 assimilation of urea in the enzyme urease and serves as the center of a nickel superoxide
51 dismutase enzyme [Dupont et al., 2008; Sunda, 2012; Broering et al., 2013; Twining and Baines,
52 2013]. Nickel has been found to be co-limiting with nitrogen under laboratory conditions [Price
53 and Morel, 1991] and is implicated in the limitation of nitrogen fixation [Ho, 2013], which is of
54 particular interest in areas like the Arctic Ocean that are nitrogen limited [Taylor et al., 2013;
55 Rijkenberg et al., 2018]. While Ni speciation has been studied much less than metals such as iron
56 and Cu, 10-60% of Ni has been reported to be bound by organic ligands [Donat et al., 1994;
57 Saito et al., 2004; Vraspir and Butler, 2009]. Unlike some other nutrient-type metals, Ni appears
58 to have both shallow and deep water regeneration, similar to both phosphate and silicate,
59 respectively [Sclater et al., 1976; Böning et al., 2015], which perhaps points to the important role
60 of diatom activity in controlling Ni’s global distribution and relationship to macronutrients
61 [Twining and Baines, 2013; Böning et al., 2015; Middag et al., 2020]. Beyond biological uptake
62 and regeneration, the inputs of Ni to the ocean are not well constrained, although continental
63 margin and river sources have been suggested to play a significant role [Westerlund et al., 1986;
64 Bowie et al., 2002; Cameron and Vance, 2014; Little et al., 2020].
65 Because of their different profile shapes and biogeochemical controls, Cu and Ni are not
66 often compared directly in oceanographic investigations. Some early studies of trace metals
67 established global baselines of multiple trace metal distributions and so did compare Cu and Ni

alongside other nutrient-type elements such as cadmium (Cd) and Zn [Bruland, 1980; Boyle et al., 1981; Dickson and Hunter, 1981; Spivack et al., 1983; Danielsson et al., 1985; Nolting and de Baar, 1994; Yeats et al., 1995; Noriki et al., 1998], but these studies rarely juxtaposed Cu and Ni directly. Notably, Cu and Ni have both been observed to be complexed by coastal organic matter [Gerringa et al., 1991; Abualhaija et al., 2015; Whitby and van den Berg, 2015] and, as divalent metals, may compete for similar ligand groups in the open ocean [Boiteau et al., 2016]. A comparison of the two could provide insight into the relative importance of biological and physicochemical processes in shaping their respective distributions, as both share riverine and continental sources [Böning et al., 2015; Richon and Tagliabue, 2019] and some nutrient-like dynamics.

The Arctic Ocean is a unique ocean basin in which to study trace metal cycling because it is more dominated by continental shelf area (>50%, [Jakobsson et al., 2004]) and riverine fluxes [Ekwurzel et al., 2001] than any other ocean basin. Additionally, the Arctic Ocean is a point of mixing between the North Atlantic and North Pacific Oceans, which have starkly different trace metal signatures [Sunda, 2012; Gerringa et al., 2021]. Prior studies of trace metals in the Arctic have noted high Cu, Ni, and other trace metal concentrations in surface and subsurface waters [Moore, 1981; Yeats, 1988; Yeats and Westerlund, 1991; Middag et al., 2011; Cid et al., 2012; Klunder et al., 2012b; Klunder et al., 2012a; Kondo et al., 2016; Jensen et al., 2019; Gerringa et al., 2021]. The origin of these subsurface enrichments in the Western Arctic is the Chukchi Shelf and the upper halocline water mass that exports shelf material offshore into the central Arctic [Cid et al., 2012; Kondo et al., 2016; Jensen et al., 2019], while the surface enrichment is likely due in part to the river-influenced Transpolar Drift (TPD) that bisects the central Arctic [Charette et al., 2020].

Here, we exploit these unique Arctic characteristics to distinguish the processes that control Cu and Ni biogeochemistry in the oceans. We assembled a pan-Arctic Cu and Ni dataset from the GEOTRACES GN01 section in the Western Arctic, the GEOTRACES GN04 section in the Eastern Arctic, and the GEOTRACES GN02/03 section in the Canadian Arctic (Figure 1). This dataset combines previously published Cu and Ni results from GN04 [Gerringa et al., 2021] and from the central Arctic (>84°N, upper 50m of GN01 [Charette et al., 2020]) with the full-depth, complete GN01 transect and unpublished GN02 and GN03 transects. Both Gerringa et al. [2021] and Charette et al. [2020] focused on a synthesis of multiple parameters including trace metals, nutrients, and accompanying isotopes. A pan-Arctic perspective focused solely on Cu and Ni allows us to identify the processes delivering Cu and Ni to the Arctic and diagnose why their distribution in the Arctic is so different than that in other major ocean basins.

2. Methods

2.1 Sample collection

A map of all sampling locations for this study is shown in Figure 1. Methods for the previously published dissolved Cu, Ni, nutrient, and oxygen isotope data along GN04 (PS94, 17 August to 14 October 2015) can be found in Gerringa et al. [2021]. Seawater samples were collected on the 2015 U.S. Arctic GEOTRACES GN01 cruise aboard the USCGC *Healy* between 9 August and 12 October 2015 and on the 2015 Canadian Arctic GEOTRACES GN02 and GN03 cruises aboard the CCGS *Amundsen* between 10 July and 1 October 2015.

The GN01 Western Arctic cruise originated in the North Pacific (Figure 1, Station 1) and continued through the Bering Strait northward along 170-180°W across the western Chukchi Shelf to the North Pole (“northbound”) and then back southward along 150°W to terminate again on the eastern Chukchi Shelf (“southbound”). Full depth samples were taken within the Bering

114 Strait, Chukchi Shelf, and Canada, Makarov, and Amundsen basins (Figure 1). Additionally,
115 clean near-surface samples were collected from shallow casts (1-20 m) through ice holes at select
116 stations (Stations 31, 33, 39, 42, 43, 46) north of 84°N and within the marginal ice zone.
117 The GN02 and GN03 cruises cover an area between the Labrador Sea at 56°N, through
118 Baffin Bay and the Canadian Arctic Archipelago (CAA), terminating in the Canada Basin,
119 sampling 17 full depth stations. Designated intercalibration "overlap" stations were GN01
120 Station 30 and GN04 Station 101 as well as GN01 Station 57 and GN03 Station CB4 (Canada
121 Basin) (Figure 1; Figure S1).
122 Dissolved trace metals Cu and Ni were collected on GN01 following established trace
123 metal clean GEOTRACES protocols [Cutter et al., 2010; Cutter and Bruland, 2012]. Briefly,
124 seawater was collected using a trace metal clean CTD rosette (Sea-Bird Electronics Inc.) on a
125 Vectran cable, equipped with 24 x 12 L Go-Flo bottles. The Go-Flo bottles were tripped at the
126 desired sampling depth on ascent at ~3 m/min, and upon recovery each bottle was immediately
127 moved into a clean, positive pressure sampling area and pressurized (~0.5 atm) with HEPA-
128 filtered air. Each Go-Flo bottle was fitted with a 0.2 μm AcroPak-200 polyethersulfone filter
129 capsule (Pall), and seawater was filtered into an acid cleaned 250 mL low density polyethylene
130 (LDPE) Nalgene bottle following three 10% volume rinses of the bottle, cap, and threads.
131 Samples were promptly acidified to 0.012 M hydrochloric acid (HCl) using 250 μL of Optima
132 grade HCl.
133 Similar procedures were used along GN02 and GN03 where a trace metal clean CTD
134 (Sea-Bird 911) rosette with 12 L Go-Flo bottles on a Kevlar line was used to collect all samples.
135 Seawater was filtered using the same 0.2 μm AcroPak-200 filter capsules into acid cleaned

LDPE (Bel Art) bottles. Samples were then promptly acidified to 0.012 M HCl (Baseline, SeaStar Chemicals).

2.2 Analysis

Following nine months storage, GN01 samples were pre-concentrated for dissolved Cu and Ni using a SeaFAST-pico system (ESI, Omaha, NE, USA) at Texas A&M University, coupled with an isotope dilution and standard curve method following Lagerström et al. [2013] and fully described in Jensen et al. [2020a]. A 10 mL aliquot of sample was taken up by the SeaFAST system following equilibration with ^{65}Cu and ^{62}Ni spike, subsequently buffered on-line to pH 6.2 ± 0.3, and immediately loaded onto a column containing Nobias-chelate PA1 resin. The bound metals were then back-eluted with 10% (v/v) HNO_3 (Optima, Fisher Scientific) into a 400 µL aliquot (25x preconcentration). This eluent was then analyzed promptly in medium resolution on a Thermo Element XR high-resolution inductively-coupled plasma mass spectrometer (HR-ICP-MS) at the R. Ken Williams Radiogenic laboratory at Texas A&M University.

Analysis of the GN02 and GN03 samples was carried out according to methodology established in Jackson et al. [2018]. Samples were analysed in a Class-100 clean room at the University of Victoria, British Columbia. Trace-metal extraction and preconcentration was performed using the seaFAST-pico system (ESI). The automated seaFAST system preconcentrated samples while removing the bulk seawater matrix through solid phase extraction [Lagerström et al., 2013]. For each sample 20 mL of seawater was loaded onto a Nobias-chelate PA1 resin column. The column was then rinsed with an ammonium acetate buffer solution (pH = 6.0), which was prepared by bubbling high-purity anhydrous ammonia gas through twice-distilled acetic acid with the pH adjusted by additions of NH_3 to remove the matrix. Samples

were back-eluted with 10% (v/v) HNO_3 (Baseline, SeaStar Chemicals, Sidney, BC, Canada) into a 2.5 mL aliquot (8x preconcentration). The preconcentrated samples were subsequently analysed using an Agilent 8800 ICP-MS/MS.

The results from the intercalibration exercise among these four cruises show significant and strong agreement between laboratories and analysis methods for both dissolved Cu and Ni across all depths, indicating that data from all three labs can be compared directly with confidence (Figure S1). Accuracy, precision, procedural blanks, and limits of detection of these measurements are summarized in Table 1.

2.3 Hydrographic and nutrient analyses

Salinity, silicate, and other macronutrients collected along GN01 were determined onboard by the Scripps Institute of Oceanography Ocean Data Facility (SIO ODF) team. Parameters such as temperature and pressure were taken directly from the trace metal CTD (Sea-Bird 911+) sensors. Bottle salinity from trace metal GoFlo bottles was measured using a Guildline Autosal 8400B salinometer. Dissolved macronutrients phosphate, and silicate were analyzed on a SEAL Analytical AutoAnalyzer 3 [Hydes et al., 2010].

Along GN02 and GN03, macronutrient samples were collected directly from the rosette and analyzed onboard on a Bran+Luebbe AutoAnalyzer 3 following methods adapted from Grasshoff et al. [2009].

2.4 Oxygen isotope analyses and fractional water mass analysis

This study uses previously reported oxygen isotope data and fractional water mass analyses from GN01 [Newton et al., 2013; Charette et al., 2020] and GN04 (PO* method, [Bauch et al., 2011; Gerringa et al., 2021]). Along GN02/GN03, oxygen isotopic composition of freshwater was determined following the CO_2 equilibration method of Epstein and Mayeda

[1953], and freshwater endmember determination for a fractional water mass analysis utilized data for practical salinity, total alkalinity, and dissolved inorganic carbon from Eicken et al. [2002]; Rysgaard et al. [2007]; Yamamoto-Kawai et al. [2009]; Miller et al. [2011]. Note that endmembers and analyses differed among the various transects but yielded good comparison for the fractions of sea ice melt and meteoric water.

3. Hydrographic Context

The Arctic Ocean is an isolated basin, dominated by shallow continental shelves and limited in exchange with the Pacific and Atlantic Oceans via narrow and relatively shallow sills (50 and 620 m, respectively). In addition, the Arctic has year-round ice coverage, and it receives 11% of the global riverine flux despite comprising only 1% of the ocean by volume [Opsahl et al., 1999]. This leads to a large freshwater reservoir in Arctic surface waters. Subsurface water masses are dictated largely by changes in salinity, due to brine rejection during sea ice formation and the relatively isothermal nature of polar oceans.

Arctic surface waters, also known as the polar mixed layer (PML), extend approximately 0 to 50 m [Talley et al., 2011; Rudels, 2015]. In the Western Arctic (Canada and Makarov basins, Figure 1), the PML mainly comprises Pacific waters advected through the Bering Strait (50 m sill), riverine discharge, and ice melt, and along the GN01 transect it has a low salinity of 22 to 31 and a potential temperature ranging -1.8 to 1.8°C. Within the Eastern Arctic (Nansen and Amundsen basins, Figure 1), the PML is saltier due to more Atlantic water influence [Rudels, 2015]. This layer is well ventilated and well-mixed, but its low salinity establishes strong stratification from denser water below. A prominent feature of the PML is the surface TPD that brings Eastern Arctic shelf-modified river water across the central Arctic Ocean and out through the Fram Strait and Canadian Archipelago [Rudels, 2015]. The TPD is characterized

by (terrigenous) organic matter and trace metals [Charette et al., 2020] and affects GN01 Stations 30-43 and GN04 Stations 81-101, 119-130 [Gerringa et al., 2021]. For the purposes of this study, we consider the PML to extend from the surface to the sharp salinity increase, indicating the first subsurface water mass: the halocline.

The cold halocline of the Western Arctic Ocean, directly below the PML, is a unique feature formed on Arctic continental shelves as a result of brine rejection during sea ice formation [Aagaard et al., 1981]. The Canada Basin of the Western Arctic presents with a "double" halocline, due to the presence of advected Pacific waters over the Chukchi Shelf. As brine is rejected during sea ice formation on the shallow Chukchi Shelf, a cold, salty water mass forms and subducts under the PML and extends well into the Canada basin, forming the Upper Halocline Layer (UHL, S 31-33.1, ~50-150 m; [Aagaard et al., 1981; Shimada et al., 2005; Woodgate et al., 2005]). Often, the UHL is delineated by its elevated silicate (Si) > 25 μmol/kg [Jones and Anderson, 1986; Anderson et al., 2013] (Figure S2). Below this, there is a Lower Halocline Layer (LHL, S 33.1-34.7, ~150-300 m), which originates from Atlantic-derived shelf waters mixed with UHL waters [Jones and Anderson, 1986]. In contrast, the Makarov basin has a "single" halocline (S 31.0-34.3, ~50-100m) that is primarily derived from the Eurasian (Eastern Arctic) shelves mixed with some Pacific-derived waters [Rudels, 2015]. Likewise, the Amundsen Basin has a single, Eurasian-influenced halocline (S 32.7-34.7) [Rudels et al., 2004]. In the Nansen Basin (present along GN04), the halocline is formed from the advection of Atlantic water across the shelves and through the St. Anna trough, cooling and freshening such that it is situated between the PML and underlying Atlantic waters [Coachman and Barnes, 1963; Rudels, 2015].

Below the halocline, the warm intermediate Atlantic waters dominate across the entire Arctic Ocean. These layers are important because Eastern Arctic intermediate and deep waters exchange with the Nordic Seas through the Fram Strait (2600 m sill depth) and the North Atlantic via the Greenland-Scotland Ridge (620 m sill depth). The Arctic's upper Atlantic layer, called the Fram Strait Branch (FSB, ~350-800m, [Rudels et al., 2004]), has a noticeable maximum in potential temperature of $\theta > 0°C$. Below this, there is another Atlantic-derived layer known as the Barents Sea Branch, which includes waters mixed from the shallower Barents Sea [Woodgate et al., 2001; Schauer et al., 2002]. Below the Atlantic layers are the homogenous, Arctic deep waters: Canada Basin Deep Water ($S > 34.92$, $-0.55°C < \theta < -0.5°C$) and Eurasian Basin Deep Water ($34.92 < S < 34.95$, $\theta < -0.7$ °C) [Aagaard et al., 1985; Talley et al., 2011].

The Canadian Arctic Archipelago (CAA) and Baffin Bay, sampled along GEOTRACES sections GN02 and GN03 (Figure 1), represents an important outflow of Arctic waters to the North Atlantic. Pacific and Atlantic-origin waters circulate eastward within the Canada Basin, become entrained into the Beaufort Gyre (BG, GN01 Stations 48-60 and GN03 Stations CB1-4) and other cyclonic surface currents, and ultimately enter the CAA. Shallow sills at the M'Clure Strait (375 m) and Barrow Strait (125 m) prevent deep water intrusion into the CAA, but the UHL nutrient maximum characteristic of the Canada Basin can also be found throughout the CAA and into Baffin Bay. These upper ocean waters mix with Arctic outflow from the Nares Strait and eventually transit southward toward the Labrador Sea and North Atlantic.

4. Results and Discussion

4.1 Copper and Nickel in the Arctic Ocean

The major result of this study is that dissolved Cu and Ni share a remarkably similar distribution across the pan-Arctic (Figures 2 and 3) that results in their strong linear correlation

250 (dCu = [0.841 (± 0.01)]*dNi – 1.35 (± 0.05), $r^2 = 0.87$, $p < 0.01$, where the uncertainty is
251 reported as standard error in the regression, Figure 4b). This similarity between dissolved Ni and
252 Cu distributions is unique to the Arctic and contrasts with the distributions of these elements in
253 other major ocean basins in four major ways. First, Arctic Cu reaches higher concentrations than
254 found in other major ocean basins (Figure 4a). Second, Arctic profile shapes of Cu and Ni are
255 unique and do not follow the strict "hybrid-type" and "nutrient-type" profile shapes, respectively,
256 that are observed in the rest of the global ocean (Figure S3); we note that the Western Arctic also
257 has unique profile shapes of Zn [Jensen et al., 2019], Cd [Zhang et al., 2019], Co [Bundy et al.,
258 2020], Fe [Jensen et al., 2020b], and macronutrients, pointing to the unique properties of the
259 Arctic. Third, Cu and Ni in the Arctic have similar distributions (Figures 2 and 3), leading to
260 their linear correlation (Figure 4b), while instead a nonlinear "kink" is found in the Cu-Ni
261 relationship of other ocean basins (Figure 4a). Finally, both Cu and Ni concentrations are very
262 low and homogenous in Arctic deep waters. This final observation may be an important clue in
263 resolving these unique concentration patterns. The high Cu and Ni concentrations driving the
264 linear Cu-Ni relationship come from surface and intermediate waters (upper 500 m, cold colors
265 in Figure 4a), while deeper Arctic waters have low, homogenous concentrations (warm colors in
266 Figure 4a).
267 To identify the processes responsible for the unique Cu and Ni distributions and
268 correlations in the Arctic Ocean, the following sections will summarize the distribution of Cu
269 and Ni with depth, within each major water mass and geographic area of the Arctic Ocean,
270 comparing Cu and Ni with other chemical tracers that are diagnostic of various source and sink
271 terms in the Arctic.
272 **4.2.1 Surface distribution of Cu and Ni**

Arctic surface concentrations of Ni and Cu were noticeably higher than surface concentrations in the Atlantic and Pacific (Figure 4a, S4). Average surface concentrations and standard deviations (±1SD) across all four transects in the upper 20m are shown in Table 2. All four Arctic transects synthesized here had significantly higher surface concentrations than the global averages of 0.80 ± 0.64 and 3.18 ± 1.53 nmol/kg reported for surface Cu and Ni, respectively [Schlitzer et al., 2018]. Note that average surface concentrations were higher and more variable along GN01 and GN04, where highest concentrations occurred within the TPD [Charette et al., 2020; Gerringa et al., 2021]. Additionally, the Cu-Ni relationship was strong in the surface waters 0-20 m depth across all four cruises (dCu = [0.95 (±0.03)]*dNi – 1.53 (±0.18), $r^2 = 0.88$, $p < 0.01$, Table 2). The correlation between Cu or Ni and salinity (Figure 5) suggests that freshwater inputs are an important source for both metals. What processes are responsible for these uniquely high surface concentrations? We test and evaluate below three hypothesized fluxes: sea ice melt, riverine fluxes, and continental shelf inputs.

4.2.2. Sea ice melt in the Marginal Ice Zone (MIZ)

Sea ice melt has the potential to be a large source of trace metals to surface seawater [Hölemann et al., 1999; Measures, 1999; Aguilar-Islas et al., 2008; Tovar-Sánchez et al., 2010; Lannuzel et al., 2016], as sea ice can deliver metals and nutrients accumulated in brine channels or carried in ice-rafted sediments [Measures, 1999] from the continental shelves to anywhere in the Arctic where ice is melting [Kadko et al., 2016; Krumpen et al., 2019]. Concentrations of Cu and Ni in Arctic sea ice have a wide observed range, from 10.7 to 430 nmol/kg and 1 to 830 nmol/kg, respectively [Hölemann et al., 1999; Tovar-Sánchez et al., 2010; Marsay et al., 2018], which could thus act as a source or a diluent of surface Arctic seawater dissolved Cu and Ni concentrations upon melting. Notably, the sea ice Cu and Ni concentrations measured on the

GN01 cruise were on the very low end, at or below this range [Marsay et al., 2018]: 0.67 ± 0.44 nmol/kg for Cu and 0.75 ± 0.47 nmol/kg for Ni. Both are significantly lower than surface Arctic seawater concentrations, hinting that sea ice is unlikely to be the source of the high surface seawater Cu and Ni concentrations observed in this study.

Nonetheless, we employed the tracers $\delta^{18}O_{sw}$ and salinity to obtain the fraction of water contributed by sea ice melt ("f_{sim}") [Newton et al., 2013] at stations designated within the "marginal ice zone" along GN01 (MIZ, Stations 8-17, 51-57), defined as stations where ice was present but coverage was <100%. Nickel had a negative relationship with f_{sim} (Figure 6d, r^2 = 0.87, $p < 0.01$, pink dots), indicating that sea ice melt acted as a diluent rather than a source to surface waters. Indeed, the extrapolated sea ice concentration of Ni was indistinguishable from zero (0.18 ± 0.94 nmol/kg), which is within the range quoted above [Marsay et al., 2018]. There was no relationship between f_{sim} and Cu, likely due to Stations 8 and 9 over the Chukchi Shelf, which are known to receive shelf sediment fluxes that could affect the relationship of metals to sea ice melt along this transect [Jensen et al., 2019] (Figure 6c, red circles). Along GN03 in the same geographic region, high surface f_{sim} values yielded a positive correlation with Cu ($r^2 = 0.72$, $p < 0.01$, Figure 6c), indicating a sea ice melt source of Cu within the BG. Extrapolation to a 100% f_{sim} value suggests that sea ice in this area may have a Cu concentration of ~9 nmol/kg. For Ni, the relationship with f_{sim} appeared to be absent at these GN03 stations ($r^2 = 0.17$, Figure 6d). Therefore, sea ice melt is not the source of the surface seawater concentration maximum for Ni in the Western Arctic and in fact only serves to dilute these concentrations upon melting, but sea ice may contribute to elevated Cu concentrations near the CAA (Figure 6c). Previously published results from GN04 in the Eastern Arctic show that both Cu and Ni were also negatively correlated to f_{sim}, again indicative of dilution [Gerringa et al., 2021].

4.2.3. Riverine inputs of Copper and Nickel

The low salinity PML, where dissolved Cu and Ni concentrations were elevated (Figures 2 and 3), is attributed to the large volume of riverine freshwaters carried into the Arctic Ocean. Previous studies used the tracers $\delta^{18}O_{SW}$ and salinity to elucidate the fraction of meteoric water contribution ("f_{met}") in the surface ocean; meteoric water contains contributions from both river water and precipitation (rain or snow). As Charette et al. [2020] have discussed, the TPD carried the highest fractions of meteoric water and thus appeared to drive the correlation with f_{met} for both Cu and Ni along GN01 and GN04 (Figure 6a,b, $r^2 = 0.92, 0.83$, $p < 0.01$, respectively). The TPD receives freshwater from multiple rivers along the Siberian shelves, but nevertheless presents a remarkably cohesive relationship among Ni, Cu, and f_{met}, as well as Cu/Ni, in the central Arctic. In fact, when the overall relationship between f_{met} and Cu and Ni is extrapolated to 100% meteoric water, a riverine end-member concentration of 22 nmol/kg for Cu and 23 nmol/kg for Ni is calculated, which is within the range of the currently known Eurasian Arctic river endmembers (~3-38 and ~4-23 nmol/kg, respectively, summarized in Table S1). Thus, the TPD plays a driving role in the observed surface maxima of Cu and Ni and the pan-Arctic linear relationship between Cu and Ni.

A recent study along the GN04 transect noted that there may be distinct plumes from the Lena River water and Yenisei/Ob River water that can be differentiated using εNd values within the TPD [Paffrath et al., 2021]. The less saline, and more radiogenic, Lena River-influenced (~0-30m) water overlies saltier, less radiogenic, Yenisei/Ob water (~50-100m). While Cu and Ni vs f_{met} slopes showed some subtle variation within the TPD water mass, as observed by Gerringa et al. [2021], they were also both negatively correlated to εNd in this study ($r^2 = 0.64$ and 0.58, respectively, $p < 0.01$, Figure S5). This suggests that the Lena River may contribute slightly

342 higher Cu and Ni compared to the underlying Yenisei/Ob Rivers. However, concentrations in
343 these rivers and estuaries were similar in range and magnitude (Table S1), and thus the different
344 riverine sources for these dissolved metals could not be distinguished clearly.
345 In this study, Cu and Ni were also elevated in surface waters outside of the TPD (Figure
346 6a,b). The surficial BG also holds a significant freshwater reservoir [Proshutinsky et al., 2009].
347 Interestingly, although f_{met} was elevated in the BG, there was no significant linear relationship
348 between f_{met} and either Cu or Ni ($r^2 = 0.34$, $r^2 = 0.006$, respectively, Figure 6a,b). Although
349 riverine fluxes make up a large component of the BG freshwater inventory, low salinity Pacific-
350 derived waters flowing through the Bering Strait are another important source of freshwaters to
351 the BG [Carmack et al., 2008]. The Yukon River outflow is entrained in the northward flowing
352 Alaskan Coastal Waters that tightly hug the western Alaskan coast and contribute to the Canada
353 Basin UHL as well as the BG. This is especially true when atmospheric conditions lead to a
354 negative Arctic Oscillation index and thus allow for a more expansive BG [Steele et al., 2004],
355 as was seen in the years preceding 2015. In fact, the concentrations of Cu and Ni in the BG were
356 similar to those found along the Bering Strait, Chukchi Shelf, and in the UHL (Figure 7),
357 suggesting that Pacific-derived water entrained into the BG may have influenced the
358 concentrations. Scavenging or biological uptake of Cu and Ni could play a role in keeping
359 concentrations uniform, as has been suggested for other geochemical tracers in the same region
360 [Guay et al., 2009]. Even at stations close to the CAA where the Mackenzie River outflow is
361 often observed, there was very little meteoric water contribution. Overall, meteoric water did not
362 appear to play a controlling role in the distribution of Cu and Ni within the BG or within water
363 entering the CAA.

The Chukchi Shelf stations had overall low f_{met} and lower concentrations of Cu and Ni (Figure 6a,b), despite the known presence of the Yukon River outflow near Stations 2 and 3 (Figure 1). For Ni, the overall Arctic f_{met} relationship was driven primarily by the TPD samples (Figure 6), while Ni was not correlated to f_{met} along the Chukchi Shelf (Figure S6b) or within the BG. Copper, in contrast, did display correlations to f_{met} along the Chukchi Shelf (Figure S6a), as well as within the TPD, indicating that riverine fluxes are particularly critical for setting surface Arctic Cu distributions. This is in line with what we know about the role of organic ligands in stabilizing Cu, particularly in estuarine environments [Laglera and van den Berg, 2003; Abualhaija et al., 2015; Whitby and van den Berg, 2015]. Previous studies in the Arctic highlight the role of terrestrially-derived humic substances entering the Arctic via the TPD as well as other river sources in controlling Fe distribution and speciation [Slagter et al., 2017; Laglera et al., 2019; Slagter et al., 2019]. Given that up to 69% of dissolved Cu may be bound by these humic substances [Abualhaija et al., 2015], we suggest that river-derived organic matter may be preferentially binding Cu, compared to Ni. Similar ligands bind Ni(II) and Cu(II) in marine and estuarine environments, but Cu(II)-humic complexes are more preferred following the Irving Williams Series [Irving and Williams, 1953], and Cu will outcompete Ni for stronger ligands [Boiteau et al., 2016]. Based on these results, Cu appears to be controlled more significantly by riverine fluxes than does Ni, and rivers are likely the dominant driver of the increase in Cu moving from the North Pacific (GN01 Station 1) through the Bering Strait and Chukchi Shelf. Increased phytoplankton uptake of Ni compared to Cu may also account for the decoupling of Ni and Cu in surface waters and is discussed below.

4.2.4. Modifications across the Chukchi, Barents, and CAA continental shelves

386 The third potential Cu and Ni surface source that we investigated was benthic fluxes from
387 the Bering Strait, Chukchi, CAA, and Barents continental shelves. While Figure 6 provides
388 strong evidence of riverine influence, the Chukchi Shelf and CAA stations showed substantial
389 deviation from the pan-Arctic Cu and Ni linear relationship shown in Figure 4b, as well as the Ni
390 vs f_{met} relationship in Figure 6b. An examination of the Bering and Chukchi Shelf Cu and Ni
391 distributions during GN01 showed that along the transect, northward from the North Pacific "end
392 member" at Station 1 across the Bering Strait and Chukchi Shelf, both Cu and Ni concentrations
393 increased in surface waters (Figure 7, S4). This surface increase was most noticeable for Cu,
394 which increased by ~2 nmol/kg from Station 1 (1.84 ± 0.09 nmol/kg) to the Chukchi Shelf break
395 at stations 8 and 61 (3.89 ± 0.53 nmol/kg). Copper concentrations at each of these shelf stations
396 were constant with depth (Figure 7a, inset). Dissolved Ni did not appear to increase significantly
397 along the shelf from ~5.0 nmol/kg at Pacific Station 1 to 5.5-6.0 nmol/kg at the shelf break
398 (Figure 7b). However, there were two features of the Ni distribution over the shelf that
399 distinguish it from the distribution of Cu. First, Ni did not follow Cu's more successive
400 northward increase. Second, Ni profiles were not constant with depth (Figure 7b, inset) and
401 instead increased significantly towards the bottom, sometimes with gradients of 2-3 nmol/kg Ni
402 between surface and bottom waters over the shelf (Figure 7b). This disparity over the shelf
403 translated to a breakdown of the otherwise linear Cu-Ni relationship (Figure S6c), despite both
404 elements increasing in concentration relative to Pacific waters, suggesting distinct controlling
405 processes over the shelf.
406 Copper is traditionally thought to have a benthic source [Boyle et al., 1981; Richon and
407 Tagliabue, 2019], and Ni can be released from sediments during diagenetic remobilization from
408 the reduction of Mn oxide phases and other mineral transformations [Little et al., 2020] or the

409 regeneration of organic matter below the sediment-water interface. Under mildly reducing
410 conditions, dissolved Cu may have a benthic, continental shelf source [Heggie, 1982; Heggie et
411 al., 1987], while under euxinic conditions, Cu precipitates in sediments as an inorganic sulfide
412 [Biller and Bruland, 2013]. Previous studies have established that benthic fluxes from the
413 Chukchi Shelf can control trace metal distributions in the rest of the Western Arctic in two
414 distinct ways: elements such as dissolved Fe, Mn, and Co are supplied by reductive dissolution
415 of Chukchi Shelf sediments [Aguilar-Islas et al., 2013; Kondo et al., 2016; Vieira et al., 2019;
416 Bundy et al., 2020; Jensen et al., 2020b], while dissolved Zn and the macronutrients are supplied
417 by porewater fluxes of remineralized Zn-rich organic matter [Jensen et al., 2019]. A principal
418 component analysis done by Vieira et al. [2019] along the Chukchi Shelf showed a relationship
419 between Ni, Zn, and the macronutrients, while Cu was not strongly correlated to either Ni, the
420 macronutrients, or Fe and Mn. We compare our Cu and Ni data to the distributions of each of
421 these metals along the Chukchi Shelf to elucidate which of these mechanisms might be driving
422 benthic fluxes of Cu and Ni.
423 Chukchi Shelf sediment porewaters are low in oxygen, creating a reducing environment
424 that remobilizes redox-active metals such as Fe, Mn, and Co [Vieira et al., 2019; Jensen et al.,
425 2020b]. However, Cu did not share a strong correlation with Fe or Mn that did have a reductive,
426 benthic source. Likewise, Cu was not correlated to the major macronutrients along the shelf in
427 this study. In fact, Cu had a significant correlation only to f_{met} along the shelf (Figure 6a, S6a),
428 suggesting that river input may be responsible for the Cu distribution along the Chukchi Shelf.
429 Dissolved Ni was moderately correlated with Zn along the Strait and Shelf stations (r^2 =
430 0.72, $p < 0.01$, Figure S7d). Like Zn, Ni was also correlated at these sites with the macronutrient
431 silicate (Si, $r^2 = 0.60$, $p < 0.01$, Figure S7e), which is known to be released during the dissolution

of diatoms in sediments along the Chukchi Shelf alongside Zn [Jensen et al., 2019], suggesting that the Ni flux from sediments was also driven by regeneration of exported phytoplankton detritus. This is consistent with a greater Ni demand of diatoms compared to other phytoplankton groups [Twining et al., 2012], which might produce a Zn and Ni flux from Chukchi Shelf sediments following regeneration in porewaters or at the sediment-water interface. While riverine input may also have a role in surface Ni concentrations on the Chukchi Shelf, any correlation with f_{met} is overshadowed by the non-conservative biological cycling affecting Ni and other bioactive metals such as Zn, Cd, and Fe in the productive Chukchi Sea [Jensen et al., 2019; Zhang et al., 2019; Jensen et al., 2020]. Thus, benthic fluxes and potential preferential uptake by phytoplankton in the surface ocean appeared to drive the distribution of Ni over the Bering and Chukchi Shelves, in contrast to Cu.

The deeper CAA stations along GN02 and GN03 (~400m) and the Barents Shelf (~200m) along GN04 did not show benthic sources or appreciable increases of either Cu or Ni (Figures 2 and 3). Gerringa et al. [2021] found no evidence for sedimentary sources of Cu or Ni along the Barents Shelf during GN04, and any increase of Cu or Ni was surficial and could be attributed to low salinity and thus riverine sources. As has been previously postulated, the Barents Shelf is less productive and may be too deep to generate a significant benthic trace metal source [Sakshaug, 2004; Jensen et al., 2019]. Sediment resuspension, rather than reductive dissolution, has been linked to Fe and Mn benthic fluxes along the CAA [Colombo et al., 2021], but this apparently did not meaningfully affect Cu and Ni, which shared no relationship to other dissolved trace metals in the CAA. The dominant feature in the CAA appeared to be the high dissolved Cu and Ni concentrations in the Canada Basin UHL waters that flow through the CAA and out into Baffin Bay.

4.3 Halocline (UHL)

Concentrations of Cu and Ni were elevated not only in the surface but also throughout the UHL observed along GN01 in the Canada Basin and into the CAA along GN03 and GN02 (Figures 2,3,7), similar to previous findings [Cid et al., 2012; Kondo et al., 2016; Jensen et al., 2019; Jensen et al., 2020b]. Within the UHL, Cu averaged 3.74 ± 0.26 nmol/kg, which was lower than its surface concentrations directly above (4.25 ± 0.29 nmol/kg; Figure 6a). In contrast, Ni averaged 7.08 ± 0.32 nmol/kg in the UHL of the Canada Basin, which was on average slightly higher than its surface average (6.73 ± 0.33 nmol/kg; Figure 6b). These UHL averages were within error of Chukchi Shelf bottom water concentrations (Figure 7), suggesting a connection between the shelf and concentrations offshore in the UHL. The UHL is formed from salty waters released during sea ice formation and brine rejection on the Chukchi Shelf [Shimada et al., 2005; Woodgate et al., 2005], which imparts high macronutrient and trace metal concentrations from shelf bottom waters that remain relatively undiluted during transit offshore [Jensen et al., 2019; Zhang et al., 2019; Jensen et al., 2020b].

The apparent increase in Ni but not Cu in the UHL compared to shelf bottom waters caused a deviation in the linear correlation between Cu and Ni at UHL depths (Figure 4b). Dissolved Cu and Ni were not significantly correlated in the UHL, with Ni positively correlated to the UHL tracer Si ($r^2 = 0.61$, $p < 0.01$, Figure S7e), while Cu was not correlated to Si (Figure S7b). This Cu-Ni decoupling could occur either because Ni and Si are sourced together from the regeneration of phytoplankton detritus in Chukchi Shelf sediments without Cu (as suggested above) and/or that Cu is scavenged away in the UHL.

Thus, we tested the hypothesis that Cu is scavenged from the UHL layer during transport using a similar calculation as previous work that has shown rapid exponential scavenging of

dissolved and particulate Fe and Mn near the shelf [Aguilar-Islas et al., 2013; Jensen et al., 2020b]. Silicate is constant with distance from the shelf break, indicating that it is not net regenerated nor scavenged. Thus, we compared averaged Cu or Ni within the bounds of the halocline (Si > 25 μmol/kg, salinity 31.0-33.1) at each of GN01 Stations 8-19, 46-60 to its distance from the 100 m isobath. Like Si, the results were approximately constant for each metal within error (Figure 8a,c), indicating that there was no substantial scavenging removal of Cu or Ni in the GN01 UHL within ~1000 km of the Chukchi Shelf break. Thus, the observation above (3.2.4) that the Chukchi Shelf provides a benthic source of Ni but not Cu is likely most responsible for the slight decoupling of Cu and Ni within the UHL.

We further probed the potential for scavenging by examining the persistence of both Cu and Ni within Pacific-origin water of the CAA. As has been observed previously, stations in the Canada Basin (CB2-CB4), the M'Clure Strait (CB1, Figure 1), and CAA have subsurface Si and trace metal maxima (Figure 3) commensurate with Canada Basin UHL water [Jackson, 2017; Lehmann et al., 2019; Colombo et al., 2020]. Along GN02 and GN03, flow within the CAA was primarily eastward from M'Clure Strait to Baffin Bay, maintaining the UHL Si maximum between salinity 31.0 and 33.1. Dissolved Cu and Ni remained elevated in this water mass with average concentrations of 3.69 ± 0.20 nmol/kg and 6.89 ± 0.44 nmol/kg, respectively, between stations CB1-4 and CAA3-CAA8 where Si is > 20 μmol/kg. However, UHL flow is known to recirculate within Barrow Strait, and therefore we truncated our UHL trends at GN03 Station CAA8, eastward of which Si was too low to distinguish the UHL. From the Chukchi Shelf 100 m isobath (Station 61) to CAA8 (1675 km total distance), Cu decreased linearly ($r^2 = 0.63$, $p < 0.01$, Figure 8b) when plotted against distance, corresponding to a removal of 0.00021 nmol/kg Cu km^{-1}. Nickel had no relationship to distance but clearly decreased between stations CAA3-

CAA7 (>2000 km from the 100m isobath, Figure 8d, grey circles), as did Cu (Figure 8b). Silicate is shown as a comparison, demonstrating a relatively conservative pattern within the Canada Basin (Figure 8e) and a similar decrease between CAA3-CAA7 (Figure 8f, grey circles) due to conservative mixing. Thus, slow scavenging of Cu within the CAA (up until Station CAA8) may be responsible for the Cu decrease moving from the Canada Basin to Baffin Bay (Figure 4), while Ni and Si were only affected by conservative mixing.

4.4 Atlantic layer (AL)

Below the halocline, the Atlantic layer (AL, ~250-600 m depth) originates in the Atlantic Ocean, flowing first through the Eastern Arctic and cycling slowly into the Western Arctic, traceable by a maximum in potential temperature (>0°C, [Rudels, 2015]). Tracking the inventory of Cu and Ni within this water mass as it ages allowed a distinction between conservative mixing of water masses (linear relationship with θ_{max} at each station), inputs of Cu and Ni (curved upward relationship with θ_{max}) such as by vertical biological regeneration inputs, or scavenging losses of Cu or Ni (curved downward relationship with θ_{max}). Previous studies found that nutrient-type metals such as Zn and Cd had a linear negative correlation with θ_{max} along GN01, indicating conservative mixing of low-Zn and –Cd Atlantic waters with the Zn- and Cd-rich halocline above [Jensen et al., 2019; Zhang et al., 2019]. Given that Ni and Cu were elevated within the Western Arctic UHL, we expected a similar linear relationship to that observed for Zn and Cd.

Using data from GN01 and GN04 (Figure S8), we observed a flat linear relationship between Ni and θ_{max} (with two outliers), indicating no non-conservative additions to or losses from the Atlantic Layer and similar Ni concentrations in the UHL and AL. Notably, along GN04, where Atlantic water was a large component of water along the Barents Shelf and Nansen Basin

524 [Gerringa et al., 2021], the θ_{max} was significantly higher (1-9°C) than at GN01 stations that were
525 composed of older Atlantic waters already mixed with colder waters above or below.
526 However, the Cu trends in the AL were more complex. There was a negative linear
527 relationship between Cu and θ_{max} along GN01 (Figure S8, blue dots), indicating conservative
528 mixing between the high-Cu UHL waters and low-Cu Atlantic waters in the Western Arctic.
529 However, the low-Cu AL trend was not borne out by the GN04 dataset, which when combined
530 with the GN01 AL data recorded no relationship between Cu and θ_{max} ([Gerringa et al., 2021];
531 Figure S8, blue and orange dots). Overall, these trends suggest that Cu and Ni are not
532 appreciably scavenged or regenerated in the AL along the circulation pathway moving from the
533 origin in the Barents Sea to the Chukchi Shelf. Importantly, a linearly decreasing relationship
534 between AOU and θ_{max} was reported previously for the GN01 stations [Jensen et al. 2019],
535 which underscores the minimal impact of vertical regeneration inputs for macronutrients or the
536 micronutrients were study here; this is most likely explained by the oligotrophic conditions under
537 the ice cover of the central Arctic [Cai et al., 2010; Black, 2018].
538 **4.5 Deep waters**
539 Concentrations of Cu and Ni were low and homogenous in deep waters below 1800 m,
540 with Cu = 1.57 ± 0.47 nmol/kg and Ni = 3.40 ± 0.35 nmol/kg across the entire Arctic (Table 3).
541 These were the lowest concentrations along all four Arctic GEOTRACES sections and represent
542 a clear contrast to global averages for deep water Cu and Ni concentration below 1000 m, which
543 are higher at 2.60 ± 1.02 nmol/kg and 7.76 ± 1.56 nmol/kg, respectively [Schlitzer et al., 2018].
544 In Arctic deep waters, Cu and Ni concentrations encompass a range too small to allow a
545 significant linear relationship between Cu and Ni below 1800 m; however, these low

546 concentrations do appear to “anchor” the overall GN01 Cu-Ni linear correlation in the Arctic
547 (Figure 4).

548 Although deep water concentrations of Cu and Ni were low overall, they did vary slightly
549 among the different Arctic Ocean basins: the Canada and Makarov basins (Western Arctic), and
550 the Nansen and Amundsen basins (Eastern Arctic). The Lomonosov Ridge prohibits significant
551 exchange between the Amundsen and Makarov basins below its 1800 m sill, while the Alpha-
552 Mendeleev Ridge between the Makarov and Canada and the Gakkel Ridge between the Nansen
553 and Amundsen basins weakly restrict exchange below 2200 m and ~2000m, respectively
554 [Jakobsson et al., 2012]. Water is generally thought to circulate gradually from the deep Nansen
555 Basin counterclockwise into the Amundsen, Makarov, and Canada Basins [Aagaard et al., 1985].
556 Below 1800 m, both Cu and Ni were higher in the younger Eastern basins compared to the older
557 Western basins (Table 3, Figure 9, [Gerringa et al., 2021]).

558 The average Ni concentrations below 1800 m were significantly different among the four
559 basins (2-tailed *t*-tests, $p < 0.05$) suggesting that Ni appreciably decreased in the deep water
560 layers between the Nansen, Amundsen, Makarov and Canada basins. This indicates that Ni
561 concentrations decreased as water circulates slowly between the basins on the timescale of
562 centuries [Timmermans et al., 2003; Rudels et al., 2004; Tanhua et al., 2009]. For Cu, only the
563 decrease moving across the Lomonosov Ridge ($p < 0.05$) was statistically significant, and the
564 spatial trends for both elements were driven primarily by noticeably higher concentrations of
565 both Cu and Ni in the Nansen and Amundsen basins (Figure 9).

566 Arctic deep waters should be excellent indicators of metal scavenging, given their large
567 age gradient (200-500 years, [Tanhua et al., 2009]) and negligible vertical regeneration inputs
568 given limited productivity under the sea ice cover, which often otherwise complicate deep water

569 scavenging trends. Globally, Ni is thought to accumulate in deep waters with age following the
570 remineralization of nutrients with depth and subsequent accumulation as deep waters age,
571 creating distinct Ni deep water clusters at lower concentrations in the Atlantic and higher
572 concentrations in the Pacific (Figure 4a). Arctic deep waters showed the opposite trend between
573 Ni, Cu, and water mass age, namely that Ni and Cu both decreased with increasing age. Recent
574 studies attribute this decrease in Ni and Cu concentration between the Eastern Arctic and
575 Western Arctic to potential boundary scavenging and the presence of shelf ventilation in the
576 Eastern Arctic [Gerringa et al., 2021]. Indeed, the Chukchi Shelf and Western Arctic stations
577 (GN01 and GN03) are more highly stratified, as evidenced by lower surface density and higher
578 Brunt-Vaisala frequencies compared to the Barents Sea and Nansen Basin stations (GN04,
579 Figure S9). This stratification in the Western Arctic likely provides a barrier to vertical
580 convection in the shelf-slope region and thus to significant mixing of high nutrient/metal UHL
581 waters into the Canada and Makarov basin deep waters.
582 Both Cu and Ni showed statistically significant differences between the younger, more
583 ventilated Eastern Arctic basins (Nansen and Amundsen, 150-200 years) and the older, more
584 stratified Western Arctic basins (Makarov and Canada, 300-500 years) [Schlosser et al., 1994;
585 Tanhua et al., 2009]. Is this due to scavenging on the timescale of centuries? While this might be
586 expected for Cu, Ni is not typically considering a scavenging-type element. We note that other
587 elements (e.g. Cd [Zhang et al., 2019], Fe, Mn, Co, Zn [Jensen et al., 2019; Bundy et al., 2020;
588 Jensen et al., 2020b; Gerringa et al., 2021]) also showed a decrease in deep water concentrations
589 across basins, and since some of these elements are also not thought to be particle-reactive, we
590 cannot definitively attribute this apparent loss of Cu or Ni to scavenging with age. Rather,
591 differences in initial water mass composition during the mixing of waters that ultimately form

Arctic deep water may help explain this trend, as has been proffered to explain Arctic deep water Si trends [Brzezinski et al., 2021] or shelf-slope ventilation as proposed in the Eastern Arctic [Gerringa et al., 2021].

Moreover, both Cu and Ni were affected by benthic nepheloid layers (BNLs) that were intermittently present along the GN01 transect. Although most full-depth stations (14, 19, 26, 30, 32, 38, 48, 52, 57) showed evidence of BNLs via a reduction in light transmission in the sensor data [Gardner et al., 2018], particulate aluminum in the large size fraction, a chemical metric of BNL lithogenic sediment resuspension, was particularly elevated at Stations 14, 19, 26, 30, 32, 48, and 57 [Xiang and Lam, 2020]. At these stations, Cu and Ni both showed variations in the bottom-most samples. At Stations 30, 32, 48, and 57, dissolved Cu decreased, and Ni increased sharply in the BNL (Figure S10), showcasing the common dynamic of benthic nepheloid layers (BNLs): scavenging of dissolved Cu [Sherrell and Boyle, 1992; Jacquot and Moffett, 2015] and resuspension-driven additions of nutrient-type elements like Ni [Sherrell and Boyle, 1992; Löscher, 1999]. In contrast, at stations 14, 19, and 26, dissolved Cu was slightly elevated near the bottom, indicating potential release from resuspended sediments [Boyle et al., 1977], while Ni appeared to decrease towards the seafloor. This could be a result of Ni scavenging onto central Arctic Mn-rich sediments [März et al., 2011], as positively charged Ni in seawater [Byrne, 2002] is expected to adsorb onto the slightly negatively-charged surfaces of Mn oxides moreso than organically-bound Cu, which prefers Fe oxide surfaces [Koschinsky and Hein, 2003]. A further analysis of spatial differences in either removal or addition of dissolved Cu and Ni in the BNLs along GN01 requires a more detailed spatial survey of Arctic sediment geochemistry, particularly the distribution of Mn vs Fe oxides in sediments that might locally and differentially scavenge these metals.

5. Conclusions

Dissolved Cu and Ni display a globally unprecedented linear relationship across the Arctic Ocean that reflects the unique fluxes into this basin and the unique distributions of trace metals. The profile shapes for Ni and Cu are noticeably different in the Arctic than in other ocean basins, with high surface concentrations far surpassing global averages and a decrease with depth to low and homogenous concentrations below 1000 m. This aligns well with studies of other metals in the Western Arctic, in particular Mn and Co, both of which have a similar profile shape to Cu and Ni [Bundy et al., 2020; Jensen et al., 2020b], as well as metals in the Eastern Arctic [Gerringa et al., 2021], pointing to Arctic-specific fluxes and water mass advection and mixing that form these unique metal distributions.

We conclude that the linear correlation between Cu and Ni across the pan-Arctic is driven predominantly by significant riverine fluxes for both Cu and Ni, particularly within the TPD. Rivers must be considered in any oceanic model of Cu or Ni biogeochemistry. In addition, we discovered that benthic porewater fluxes associated with the sediment regeneration of organic matter are also an important source for Ni into bottom waters of the Bering and Chukchi Shelves along GN01, which are eventually entrained into the UHL of the open Western Arctic. In contrast, Cu showed no benthic margin source or evidence of surface biological uptake and instead remained correlated to river input. This is opposite to the pattern expected from previous investigations, where benthic sources have long been considered for Cu but were underemphasized for Ni. However, riverine and benthic sources are particularly prevalent in the Western Arctic Ocean, with significant freshwater volume accumulation in surface waters [Carmack et al., 2008; Yamamoto-Kawai et al., 2008] and on the shallow Chukchi Shelf [Jakobsson et al., 2004]. The TPD bisecting the Arctic is also a notable feature for trace metals in

638 the surface Makarov and Amundsen basins [Charette et al., 2020]. In particular, our conclusion
639 that the riverine fluxes are the dominant control on Cu in the PML in this region aligns well with
640 current literature suggesting that the river flux of Cu is far greater and more dominant than
641 previously established, decreasing the residence time of Cu in the ocean considerably [Richon
642 and Tagliabue, 2019].

643 Removal by scavenging in surface and intermediate waters such as the UHL or Atlantic
644 layer appears possible for Cu only within the CAA and was not observed for Ni. Previous work
645 shows removal of non- scavenged-type elements in the Arctic deep waters, in line with the
646 observation of this study that dissolved Cu and Ni concentrations decreased across the four Arctic
647 basins with increasing age over century timescales. While this may be due to shelf-slope
648 ventilation or changes in initial water mass concentrations that mixed in these basins during deep
649 water formation, scavenging of both Cu and Ni cannot be precluded by our deep water
650 observations, and it is notable that Ni scavenging has been hypothesized to occur onto Mn oxides
651 [Koschinsky and Hein, 2003] and in the Mediterranean Sea [Middag et al., 2022].

652 More work is needed on Arctic Cu and Ni distributions, as well as the chemical
653 complexation of Cu and Ni, to demonstrate whether this coupled Cu-Ni behavior is merely a
654 reflection of processes endemic to the Arctic Ocean where freshwater sources are dominant and
655 vertical biological pump processes are weak. Indeed, there were no discernable effects from
656 biological uptake and remineralization across the Arctic basins and within the CAA off-shelf.
657 Given the impact of river outflow on Cu and Ni concentrations, we may expect increased Arctic
658 freshening to bring higher levels of Cu and Ni into the surface Arctic in future. Further studies
659 evaluating freshwater anomalies in the North Atlantic resulting from a freshening Arctic Ocean

should note the geochemical impact of high Cu and Ni present in Arctic rivers and productive shelves.

Acknowledgements

We would like to thank and acknowledge the Captain and crew of the USCGC *Healy*, Chief Scientists Dave Kadko, William Landing, and Greg Cutter for proposing and enabling cruise leadership, Chief Scientist Ursula Schauer and Captain Schwarze, and the crew of FS *Polarstern* on GN04, and Chief Scientist Roger François and the captain and crew of the *CCGS Amundsen.* This work would not have been possible without the GN01 Supertechnicians Gabi Weiss and Simone Moos and GN02/GN03 trace metal group (Priyanka Chandan, Kang Wang, Kathleen Munson, Jingxuan Li, David Semeniuk, Dave Janssen, Rowan Fox and Kathryn Purdon) for sample collection at sea. We thank Luz Romero for assistance with ICP-MS analyses and maintenance and Angelica Pasqualini, Bob Newton, Peter Schlosser, Tobias Koffman, Helmuth Thomas, and Alfonso Mucci for contribution of their oxygen isotope measurements and freshwater model estimates used to quantify fractional sea ice melt and meteoric water. Additionally, this work would not have been possible without the SIO ODF team for nutrient and salinity analyses during GN01. This work was supported by NSF Division of Ocean Sciences (OCE) award 1434493 and 1713677 to JNF and RMS and the NWO under contract number 822.01.018 to L.J.A. Gerringa. D. Bauch was funded for this project by DFG (BA1689/2-2).

Data Availability Statement

All dissolved metal, nutrient, and stable isotope data from GN01, GN02, GN03, and GN04 described above are available in a consolidated form as part of the GEOTRACES Intermediate Data Product 2021, available for free download at https://www.geotraces.org/geotraces-intermediate-data-product-2021/. Note that the sole exception is the macronutrient data for GN04 available at https://doi.org/10.1594/PANGAEA.868396. Individual datasets may be found at: GN01 metals (DOI:10.26008/1912/bco-dmo.817259.2), GN01 hydrography and nutrients

(DOI:10.1575/1912/bco-dmo.647259.4 and https://doi.org/10.1594/IEDA/100633), GN04 (DOI: 10.25850/nioz/7b.b.jc), GN02/03 (https://dspace.library.uvic.ca/handle/1828/8920).

Figure Captions

Figure 1. GEOTRACES Arctic GN01, GN01, GN03, and GN04 transects labeled with relevant stations, rivers, seas, and bathymetric features identified. Black dots refer to GN01, red dots GN03, white dots GN02, blue dots GN04. AB = Amundsen Basin, MB = Makarov Basin, CB = Canada Basin, LR = Lomonosov Ridge, A-MR = Alpha-Mendeleev Ridge, GR = Gakkel Ridge. An inset is included to show the detail above 85N. The yellow asterisks refer to overlap/intercalibration stations (see Figure S1).

Figure 2. Section plots of a) Cu and b) Ni across GN01 and GN04. The section is shown in the inset map beginning in the North Pacific (GN01 Station 1) and ending on the Barents Shelf (GN04 Station 173). Major basins and representative stations are also identified in panel a. Cu and Ni show a similar distribution across both transects. See Figure S2 for Si and P sections.

Figure 3. Section plots of a) Cu and b) Ni across GN01, GN02, and GN03. The section is shown in the inset map beginning in the North Pacific (GN01 Station 1) and ending in Baffin Bay (GN02 Station BB1). Major basins and representative stations are also identified in panel a. Dissolved Cu and Ni show a similar distribution across both transects. See Figure S2 for Si and P sections.

Figure 4. Dissolved Cu vs Ni concentrations a) globally (from the GEOTRACES IDP-2017) and b) within the Arctic Ocean only (GN01-03 and GN04 [Gerringa et al., 2021]). In a), the global stations are in light grey with two representative Atlantic (blue, GP02) and Pacific (red, GA03) stations highlighted to demonstrate how uniquely linear the Cu-Ni relationship is within the

712 Arctic (colored). Also, surface Arctic concentrations are high, and deep water concentrations are
713 low compared to opposite nutrient-type trends across the rest of the global ocean. In b), all Arctic
714 data are in light grey, with representative stations indicated by single colors, such as the TPD
715 (red, dark grey, black), the halocline (light and dark blue), the shelves (light and dark green), and
716 the "background" Eastern Arctic (yellow).
717 **Figure 5.** Plots of a) Cu and b) Ni vs salinity across the Arctic basin at all depths (>75°N, GN01-
718 04). Silicate is overlaid in color to indicate the UHL (UHL Si > 25 μmol/kg). Black dots indicate
719 stations where Si concentrations were not available. Note that Ni is particularly elevated in the
720 UHL. Also note that both Cu and Ni have two distinct freshwater (low salinity) metal sources: the
721 TPD (with higher Cu and Ni concentrations) and the Beaufort Gyre (with lower Cu and Ni
722 concentrations). TPD = Transpolar Drift, BG = Beaufort Gyre, UHL = upper halocline.
723 **Figure 6.** Plots of Cu and Ni vs fraction of meteoric water (a, b) and fraction of sea ice melt (c, d)
724 in surface waters (<50m). TPD = Transpolar Drift, BG = Beaufort Gyre, MIZ = Marginal Ice
725 Zone. Various linear relationships are shown in the legend (dashed or solid lines). Colors are used
726 to differentiate major geographic areas such as the shelves, the CAA, and central Arctic. Note that
727 GN04 "non-TPD" include stations 50, 54, 58, 64 outside of the TPD. GN01 Stations 8 and 9 are
728 circled in red in (c, d) to highlight their high f_{sim} values in the MIZ.
729 **Figure 7.** Profile overlay of the concentrations from GN01 of a) Cu and b) Ni across the entire
730 transect in the upper 500 m of the water column (Station 32 in Amundsen Basin excluded). A
731 grouping of Bering and Chukchi Shelf stations (Stations 2-8, 61-66, closed circle symbols)
732 demonstrate the change in Cu and Ni in the upper water column moving from Station 1 across the
733 continental shelf. Offshore there are higher Cu and Ni concentrations in the UHL of the Canada

734 Basin (Stations 14, 19, 48-57 open triangle symbols) than in the halocline of the Makarov Basin
735 (Stations 26-43, open square symbols).
736 **Figure 8.** Plots of average Cu, Ni, and Si within the UHL (elevated Si, salinity 31-33.1) vs
737 distance from the 100m isobath (shelf break) along GN01 (lefthand panels a,c,e) and GN01 into
738 GN03/GN02 (righthand panels b, d, f). Stations used in a, c, e are GN01 Stations 8-19, 46-60 and
739 in b,d,f GN01 Stations 65, 57, 60, GN03 Stations CAA8-CB4 (black dots) and GN02 Stations
740 CAA3-CAA7 (grey dots). Correlations are shown for all relationships; only panel b had a
741 statistically significant correlation between GN01 Station 60 to GN03 Station CAA8.
742 **Figure 9**. Copper and nickel in Arctic deep water. a) Cu and b) Ni below 1800m in the Canada
743 Basin (CB, GN01 Station 57), Makarov Basin (MB, GN01 Station 30, purple), Amundsen Basin
744 (AB, GN04 Station 81, red), and Nansen Basin (NB, GN04 Station 58, yellow). There is a clear
745 disparity between the Eastern (NB and AB) and Western (CB and MB) Basins, particularly for
746 Ni.
747 **Table 1.** Precision and accuracy of measurements used in this publication. Standard reference
748 materials such as SAFe D1 were used by all labs to assess the accuracy of their measurements
749 with labs reporting an average and a standard deviation based on *n* replicates. All labs were in
750 good agreement with the consensus values. Blanks and detection limits (defined as 3 x standard
751 deviation) are reported in the bottom half of the table. *originally reported in Jackson [2017] and
752 ** Gerringa et al. [2021].
753 **Table 2.** Average surface (0-20m) concentrations across all four cruise transects (GN01, GN02,
754 GN03, GN04) for Cu and Ni ± standard deviation. The global surface average is taken from
755 Schlitzer et al. [2018]. In the bottom half of the table the Cu/Ni linear relationship is reported for
756 the surface and across all four cruise transects throughout all depths. Note that GN01 Station 1

(North Pacific endmember) is excluded from all calculations within this table, as are GN02 stations K1, LS1 and LS2 (North Atlantic/Labrador Sea endmembers).

Table 3. Average deep water concentrations ± standard deviation for all four basins. The composite average and standard deviation as well as the global average are shown below for reference. Cruise transects GN01, GN03, and GN04 are included in this analysis where station depth exceeded 1800m.

References

Aagaard, K., L. Coachman, and E. Carmack (1981), On the halocline of the Arctic Ocean, *Deep Sea Research Part A. Oceanographic Research Papers*, *28*(6), 529-545.

Aagaard, K., J. H. Swift, and E. C. Carmack (1985), Thermohaline circulation in the Arctic Mediterranean Seas, *Journal of Geophysical Research: Oceans*, *90*(C3), 4833-4846.

Abualhaija, M. M., H. Whitby, and C. M. G. van den Berg (2015), Competition between copper and iron for humic ligands in estuarine waters, *Marine Chemistry*, *172*, 46-56.

Aguilar-Islas, A. M., R. D. Rember, C. W. Mordy, and J. Wu (2008), Sea ice-derived dissolved iron and its potential influence on the spring algal bloom in the Bering Sea, *Geophysical Research Letters*, *35*(24), n/a-n/a.

Aguilar-Islas, A. M., R. Rember, S. Nishino, T. Kikuchi, and M. Itoh (2013), Partitioning and lateral transport of iron to the Canada Basin, *Polar Science*, *7*(2), 82-99.

Anderson, L. G., P. S. Andersson, G. Björk, E. Peter Jones, S. Jutterström, and I. Wåhlström (2013), Source and formation of the upper halocline of the Arctic Ocean, *Journal of Geophysical Research: Oceans*, *118*(1), 410-421.

Annett, A. L., S. Lapi, T. J. Ruth, and M. T. Maldonado (2008), The effects of Cu and Fe availability on the growth and Cu: C ratios of marine diatoms, *Limnology and oceanography*, *53*(6), 2451-2461.

Bacon, M. P., and R. F. Anderson (1982), Distribution of thorium isotopes between dissolved and particulate forms in the deep sea, *Journal of Geophysical Research: Oceans*, *87*(C3), 2045-2056.

Bauch, D., M. R. van der Loeff, N. Andersen, S. Torres-Valdes, K. Bakker, and E. P. Abrahamsen (2011), Origin of freshwater and polynya water in the Arctic Ocean halocline in summer 2007, *Progress in Oceanography*, *91*(4), 482-495.

Biller, D. V., and K. W. Bruland (2013), Sources and distributions of Mn, Fe, Co, Ni, Cu, Zn, and Cd relative to macronutrients along the central California coast during the spring and summer upwelling season, *Marine Chemistry*, *155*, 50-70.

Black, E. E. (2018), An investigation of basin-scale controls on upper ocean export and remineralization, Massachusetts Institute of Technology.
Boiteau, R. M., C. P. Till, A. Ruacho, R. M. Bundy, N. J. Hawco, A. M. McKenna, K. A. Barbeau, K. W. Bruland, M. A. Saito, and D. J. Repeta (2016), Structural Characterization of Natural Nickel and Copper Binding Ligands along the US GEOTRACES Eastern Pacific Zonal Transect, *Frontiers in Marine Science*, *3*(243).
Böning, P., T. Shaw, K. Pahnke, and H.-J. Brumsack (2015), Nickel as indicator of fresh organic matter in upwelling sediments, *Geochimica et Cosmochimica Acta*, *162*, 99-108.
Bowie, A. R., D. J. Whitworth, E. P. Achterberg, R. F. C. Mantoura, and P. J. Worsfold (2002), Biogeochemistry of Fe and other trace elements (Al, Co, Ni) in the upper Atlantic Ocean, *Deep Sea Research Part I: Oceanographic Research Papers*, *49*(4), 605-636.
Boyle, E. A., F. Sclater, and J. Edmond (1977), The distribution of dissolved copper in the Pacific, *Earth and planetary science letters*, *37*(1), 38-54.
Boyle, E. A., S. S. Huested, and S. P. Jones (1981), On the distribution of copper, nickel, and cadmium in the surface waters of the North Atlantic and North Pacific Ocean, *Journal of Geophysical Research: Oceans*, *86*(C9), 8048-8066.
Broering, E. P., P. T. Truong, E. M. Gale, and T. C. Harrop (2013), Synthetic Analogues of Nickel Superoxide Dismutase: A New Role for Nickel in Biology, *Biochemistry*, *52*(1), 4-18.
Bruland, K. W. (1980), Oceanographic distributions of cadmium, zinc, nickel, and copper in the North Pacific, *Earth and Planetary Science Letters*, *47*(2), 176-198.
Bruland, K. W., R. Middag, and M. C. Lohan (2014), 8.2 - Controls of Trace Metals in Seawater, in *Treatise on Geochemistry (Second Edition)*, edited by H. D. Holland and K. K. Turekian, pp. 19-51, Elsevier, Oxford.
Brzezinski, M. A., I. Closset, J. L. Jones, G. F. de Souza, and C. Maden (2021), New Constraints on the Physical and Biological Controls on the Silicon Isotopic Composition of the Arctic Ocean, *Frontiers in Marine Science*, *8*.
Bundy, R. M., et al. (2020), Elevated sources of cobalt in the Arctic Ocean, *Biogeosciences Discuss.*, *2020*, 1-46.
Byrne, R. H. (2002), Inorganic speciation of dissolved elements in seawater: the influence of pH on concentration ratios, *Geochemical Transactions*, *3*(1), 11.
Cai, P., M. Rutgers Van Der Loeff, I. Stimac, E. M. Nöthig, K. Lepore, and S. Moran (2010), Low export flux of particulate organic carbon in the central Arctic Ocean as revealed by 234Th: 238U disequilibrium, *Journal of Geophysical Research: Oceans*, *115*(C10).
Cameron, V., and D. Vance (2014), Heavy nickel isotope compositions in rivers and the oceans, *Geochimica et Cosmochimica Acta*, *128*, 195-211.
Carmack, E., F. McLaughlin, M. Yamamoto-Kawai, M. Itoh, K. Shimada, R. Krishfield, and A. Proshutinsky (2008), Freshwater storage in the Northern Ocean and the special role of the Beaufort Gyre, in *Arctic–subArctic ocean fluxes*, edited, pp. 145-169, Springer.
Charette, M. A., et al. (2020), The Transpolar Drift as a Source of Riverine and Shelf-Derived Trace Elements to the Central Arctic Ocean, *Journal of Geophysical Research: Oceans*, *125*, e2019JC015920.
Cid, A. P., S. Nakatsuka, and Y. Sohrin (2012), Stoichiometry among bioactive trace metals in the Chukchi and Beaufort Seas, *Journal of oceanography*, *68*(6), 985-1001.
Coachman, L. K., and C. A. Barnes (1963), The Movement of Atlantic Water in the Arctic Ocean, *ARCTIC; Vol 16, No 1 (1963): March: 1–80*.

838 Coale, K. H., and K. W. Bruland (1988), Copper complexation in the Northeast Pacific,
839 *Limnology and Oceanography*, *33*(5), 1084-1101.
840 Colombo, M., S. L. Jackson, J. T. Cullen, and K. J. Orians (2020), Dissolved iron and manganese
841 in the Canadian Arctic Ocean: On the biogeochemical processes controlling their distributions,
842 *Geochimica et Cosmochimica Acta*.
843 Colombo, M., B. Rogalla, J. Li, S. E. Allen, K. J. Orians, and M. T. Maldonado (2021),
844 Canadian Arctic Archipelago Shelf-Ocean Interactions: A Major Iron Source to Pacific Derived
845 Waters Transiting to the Atlantic, *Global Biogeochemical Cycles*, *35*(10), e2021GB007058.
846 Cutter, G., P. Andersson, L. Codispoti, P. Croot, R. Francois, M. Lohan, H. Obata, and M.
847 Rutgers vd Loeff (2010), Sampling and sample-handling protocols for GEOTRACES cruises,
848 edited, GEOTRACES.
849 Cutter, G. A., and K. W. Bruland (2012), Rapid and noncontaminating sampling system for trace
850 elements in global ocean surveys, *Limnology and Oceanography: Methods*, *10*(6), 425-436.
851 Danielsson, L.-G., B. Magnusson, and S. Westerlund (1985), Cadmium, copper, iron, nickel and
852 zinc in the north-east Atlantic Ocean, *Marine Chemistry*, *17*(1), 23-41.
853 Dickson, R. J., and K. A. Hunter (1981), Copper and nickel in surface waters of Otago Harbour,
854 *New Zealand Journal of Marine and Freshwater Research*, *15*(4), 475-480.
855 Donat, J. R., K. A. Lao, and K. W. Bruland (1994), Speciation of dissolved copper and nickel in
856 South San Francisco Bay: a multi-method approach, *Analytica Chimica Acta*, *284*(3), 547-571.
857 Dupont, C. L., K. Barbeau, and B. Palenik (2008), Ni Uptake and Limitation in Marine
858 Synechococcus Strains, *Applied and Environmental Microbiology*, *74*(1), 23-31.
859 Eicken, H., H. Krouse, D. Kadko, and D. Perovich (2002), Tracer studies of pathways and rates
860 of meltwater transport through Arctic summer sea ice, *Journal of Geophysical Research:*
861 *Oceans*, *107*(C10).
862 Ekwurzel, B., P. Schlosser, R. A. Mortlock, R. G. Fairbanks, and J. H. Swift (2001), River
863 runoff, sea ice meltwater, and Pacific water distribution and mean residence times in the Arctic
864 Ocean, *Journal of Geophysical Research: Oceans*, *106*(C5), 9075-9092.
865 Epstein, S., and T. Mayeda (1953), Variation of O18 content of waters from natural sources,
866 *Geochimica et cosmochimica acta*, *4*(5), 213-224.
867 Gardner, W. D., M. J. Richardson, and A. V. Mishonov (2018), Global assessment of benthic
868 nepheloid layers and linkage with upper ocean dynamics, *Earth and Planetary Science Letters*,
869 *482*(Supplement C), 126-134.
870 Gerringa, L. J. A., J. van der Meer, and G. Cauwet (1991), Complexation of copper and nickel in
871 the dissolved phase of marine sediment slurries, *Marine Chemistry*, *36*(1), 51-70.
872 Gerringa, L. J. A., M. J. A. Rijkenberg, H. A. Slagter, P. Laan, R. Paffrath, D. Bauch, M. Rutgers
873 van der Loeff, and R. Middag (2021), Dissolved Cd, Co, Cu, Fe, Mn, Ni and Zn in the Arctic
874 Ocean, *Journal of Geophysical Research: Oceans*, e2021JC017323.
875 Granger, J., and B. B. Ward (2003), Accumulation of nitrogen oxides in copper-limited cultures
876 of denitrifying bacteria, *Limnology and Oceanography*, *48*(1), 313-318.
877 Grasshoff, K., K. Kremling, and M. Ehrhardt (2009), *Methods of seawater analysis*, John Wiley
878 & Sons.
879 Guay, C. K., F. A. McLaughlin, and M. Yamamoto-Kawai (2009), Differentiating fluvial
880 components of upper Canada Basin waters on the basis of measurements of dissolved barium
881 combined with other physical and chemical tracers, *Journal of Geophysical Research: Oceans*,
882 *114*(C1).

Heggie, D., G. Klinkhammer, and D. Cullen (1987), Manganese and copper fluxes from continental margin sediments, *Geochimica et Cosmochimica Acta*, *51*(5), 1059-1070.
Heggie, D. T. (1982), Copper in surface waters of the Bering Sea, *Geochimica et Cosmochimica Acta*, *46*(7), 1301-1306.
Hines, M. E., W. Berry Lyons, P. B. Armstrong, W. H. Orem, M. J. Spencer, H. E. Gaudette, and G. E. Jones (1984), Seasonal metal remobilization in the sediments of Great Bay, New Hampshire, *Marine Chemistry*, *15*(2), 173-187.
Ho, T.-Y. (2013), Nickel limitation of nitrogen fixation in Trichodesmium, *Limnology and Oceanography*, *58*(1), 112-120.
Hölemann, J., M. Schirmacher, and A. Prange (1999), Dissolved and particulate major and trace elements in newly formed ice from the Laptev Sea (Transdrift III, October 1995), in *Land-Ocean Systems in the Siberian Arctic*, edited, pp. 101-111, Springer.
Hydes, D., M. Aoyama, A. Aminot, K. Bakker, S. Becker, S. Coverly, A. Daniel, A. Dickson, O. Grosso, and R. Kerouel (2010), Determination of dissolved nutrients (N, P, Si) in seawater with high precision and inter-comparability using gas-segmented continuous flow analysers.
Irving, H., and R. J. P. Williams (1953), 637. The stability of transition-metal complexes, *Journal of the Chemical Society (Resumed)*, 3192-3210.
Jackson, S. (2017), The distribution of dissolved cadmium in the Canadian Arctic Ocean, Dissertation thesis, University of Victoria. http://hdl.handle.net/1828/8920.
Jackson, S. L., J. Spence, D. J. Janssen, A. R. S. Ross, and J. T. Cullen (2018), Determination of Mn, Fe, Ni, Cu, Zn, Cd and Pb in seawater using offline extraction and triple quadrupole ICP-MS/MS, *Journal of Analytical Atomic Spectrometry*, *33*(2), 304-313.
Jacquot, J. E., and J. W. Moffett (2015), Copper distribution and speciation across the International GEOTRACES Section GA03, *Deep Sea Research Part II: Topical Studies in Oceanography*, *116*, 187-207.
Jakobsson, M., A. Grantz, Y. Kristoffersen, R. Macnab, R. MacDonald, E. Sakshaug, R. Stein, and W. Jokat (2004), The Arctic Ocean: Boundary conditions and background information, in *The organic carbon cycle in the Arctic Ocean*, edited, pp. 1-32, Springer.
Jakobsson, M., L. Mayer, B. Coakley, J. A. Dowdeswell, S. Forbes, B. Fridman, H. Hodnesdal, R. Noormets, R. Pedersen, and M. Rebesco (2012), The international bathymetric chart of the Arctic Ocean (IBCAO) version 3.0, *Geophysical Research Letters*, *39*(12).
Jensen, L. T., N. J. Wyatt, W. M. Landing, and J. N. Fitzsimmons (2020a), Assessment of the stability, sorption, and exchangeability of marine dissolved and colloidal metals, *Marine Chemistry*, *220*, 103754.
Jensen, L. T., N. J. Wyatt, B. S. Twining, S. Rauschenberg, W. M. Landing, R. M. Sherrell, and J. N. Fitzsimmons (2019), Biogeochemical Cycling of Dissolved Zinc in the Western Arctic (Arctic GEOTRACES GN01), *Global Biogeochemical Cycles*, *33*(3), 343-369.
Jensen, L. T., P. Morton, B. S. Twining, M. I. Heller, M. Hatta, C. I. Measures, S. John, R. Zhang, P. Pinedo-Gonzalez, and R. M. Sherrell (2020b), A comparison of marine Fe and Mn cycling: US GEOTRACES GN01 Western Arctic case study, *Geochimica et Cosmochimica Acta*.
Jones, E. P., and L. G. Anderson (1986), On the origin of the chemical properties of the Arctic Ocean halocline, *Journal of Geophysical Research: Oceans*, *91*(C9), 10759-10767.
Kadko, D., B. Galfond, W. M. Landing, and R. U. Shelley (2016), Determining the pathways, fate, and flux of atmospherically derived trace elements in the Arctic ocean/ice system, *Marine Chemistry*, *182*(Supplement C), 38-50.

Klunder, M. B., P. Laan, R. Middag, H. J. W. de Baar, and K. Bakker (2012a), Dissolved iron in the Arctic Ocean: Important role of hydrothermal sources, shelf input and scavenging removal, *Journal of Geophysical Research: Oceans*, *117*(C4), n/a-n/a.

Klunder, M. B., D. Bauch, P. Laan, H. J. W. de Baar, S. van Heuven, and S. Ober (2012b), Dissolved iron in the Arctic shelf seas and surface waters of the central Arctic Ocean: Impact of Arctic river water and ice-melt, *Journal of Geophysical Research: Oceans*, *117*(C1), n/a-n/a.

Kondo, Y., H. Obata, N. Hioki, A. Ooki, S. Nishino, T. Kikuchi, and K. Kuma (2016), Transport of trace metals (Mn, Fe, Ni, Zn and Cd) in the western Arctic Ocean (Chukchi Sea and Canada Basin) in late summer 2012, *Deep Sea Research Part I: Oceanographic Research Papers*, *116*, 236-252.

Koschinsky, A., and J. R. Hein (2003), Uptake of elements from seawater by ferromanganese crusts: solid-phase associations and seawater speciation, *Marine Geology*, *198*(3), 331-351.

Krumpen, T., H. J. Belter, A. Boetius, E. Damm, C. Haas, S. Hendricks, M. Nicolaus, E.-M. Nöthig, S. Paul, and I. Peeken (2019), Arctic warming interrupts the Transpolar Drift and affects long-range transport of sea ice and ice-rafted matter, *Scientific reports*, *9*(1), 1-9.

Lagerström, M. E., M. P. Field, M. Séguret, L. Fischer, S. Hann, and R. M. Sherrell (2013), Automated on-line flow-injection ICP-MS determination of trace metals (Mn, Fe, Co, Ni, Cu and Zn) in open ocean seawater: Application to the GEOTRACES program, *Marine Chemistry*, *155*(0), 71-80.

Laglera, L. M., and C. M. van den Berg (2003), Copper complexation by thiol compounds in estuarine waters, *Marine Chemistry*, *82*(1-2), 71-89.

Laglera, L. M., C. Sukekava, H. A. Slagter, J. Downes, A. Aparicio-Gonzalez, and L. J. A. Gerringa (2019), First Quantification of the Controlling Role of Humic Substances in the Transport of Iron Across the Surface of the Arctic Ocean, *Environmental Science & Technology*, *53*(22), 13136-13145.

Lannuzel, D., M. Vancoppenolle, P. Van der Merwe, J. De Jong, K. M. Meiners, M. Grotti, J. Nishioka, and V. Schoemann (2016), Iron in sea ice: Review and new insights, *Elem Sci Anth*, *4*.

Lehmann, N., M. Kienast, J. Granger, A. Bourbonnais, M. Altabet, and J. É. Tremblay (2019), Remote western Arctic nutrients fuel remineralization in deep Baffin Bay, *Global Biogeochemical Cycles*, *33*(6), 649-667.

Little, S. H., C. Archer, J. McManus, J. Najorka, A. V. Wegorzewski, and D. Vance (2020), Towards balancing the oceanic Ni budget, *Earth and Planetary Science Letters*, *547*, 116461.

Löscher, B. M. (1999), Relationships among Ni, Cu, Zn, and major nutrients in the Southern Ocean, *Marine Chemistry*, *67*(1), 67-102.

Maldonado, M. T., A. E. Allen, J. S. Chong, K. Lin, D. Leus, N. Karpenko, and S. L. Harris (2006), Copper-dependent iron transport in coastal and oceanic diatoms, *Limnology and Oceanography*, *51*(4), 1729-1743.

Marsay, C. M., et al. (2018), Dissolved and particulate trace elements in late summer Arctic melt ponds, *Marine Chemistry*, *204*, 70-85.

März, C., A. Stratmann, J. Matthiessen, A. K. Meinhardt, S. Eckert, B. Schnetger, C. Vogt, R. Stein, and H. J. Brumsack (2011), Manganese-rich brown layers in Arctic Ocean sediments: Composition, formation mechanisms, and diagenetic overprint, *Geochimica et Cosmochimica Acta*, *75*(23), 7668-7687.

Measures, C. (1999), The role of entrained sediments in sea ice in the distribution of aluminium and iron in the surface waters of the Arctic Ocean, *Marine chemistry*, *68*(1-2), 59-70.

Middag, R., H. J. W. de Baar, P. Laan, and M. B. Klunder (2011), Fluvial and hydrothermal input of manganese into the Arctic Ocean, *Geochimica et Cosmochimica Acta*, *75*(9), 2393-2408.
Middag, R., H. J. de Baar, K. W. Bruland, and S. M. van Heuven (2020), The distribution of nickel in the west-Atlantic Ocean, its relationship with phosphate and a comparison to cadmium and zinc, *Frontiers in Marine Science*, *7*, 105.
Middag, R., J. M. Rolison, E. George, L. J. A. Gerringa, M. J. A. Rijkenberg, and C. H. Stirling (2022), Basin scale distributions of dissolved manganese, nickel, zinc and cadmium in the Mediterranean Sea, *Marine Chemistry*, *238*, 104063.
Miller, L. A., T. N. Papakyriakou, R. E. Collins, J. W. Deming, J. K. Ehn, R. W. Macdonald, A. Mucci, O. Owens, M. Raudsepp, and N. Sutherland (2011), Carbon dynamics in sea ice: A winter flux time series, *Journal of Geophysical Research: Oceans*, *116*(C2).
Moffett, J. W., and L. E. Brand (1996), Production of strong, extracellular Cu chelators by marine cyanobacteria in response to Cu stress, *Limnology and Oceanography*, *41*(3), 388-395.
Moffett, J. W., L. E. Brand, P. L. Croot, and K. A. Barbeau (1997), Cu speciation and cyanobacterial distribution in harbors subject to anthropogenic Cu inputs, *Limnology and Oceanography*, *42*(5), 789-799.
Moore, R. M. (1978), The distribution of dissolved copper in the eastern Atlantic Ocean, *Earth and planetary science letters*, *41*(4), 461-468.
Moore, R. M. (1981), Oceanographic distributions of zinc, cadmium, copper and aluminium in waters of the central arctic, *Geochimica et Cosmochimica Acta*, *45*(12), 2475-2482.
Newton, R., P. Schlosser, R. Mortlock, J. Swift, and R. MacDonald (2013), Canadian Basin freshwater sources and changes: Results from the 2005 Arctic Ocean Section, *Journal of Geophysical Research: Oceans*, *118*(4), 2133-2154.
Nolting, R. F., and H. J. W. de Baar (1994), Behaviour of nickel, copper, zinc and cadmium in the upper 300 m of a transect in the Southern Ocean (57°–62°S, 49°W), *Marine Chemistry*, *45*(3), 225-242.
Noriki, S., Y. Arashitani, M. Minakawa, K. Harada, and S. Tsunogai (1998), Vertical cycling of Cu and Ni in the western North and Equatorial Pacific, *Marine chemistry*, *59*(3-4), 211-218.
Opsahl, S., R. Benner, and R. M. W. Amon (1999), Major flux of terrigenous dissolved organic matter through the Arctic Ocean, *Limnology and Oceanography*, *44*(8), 2017-2023.
Paffrath, R., G. Laukert, D. Bauch, M. R. van der Loeff, and K. Pahnke (2021), Separating individual contributions of major Siberian rivers in the Transpolar Drift of the Arctic Ocean, *Scientific Reports*, *11*(1), 1-11.
Price, N., and F. M. Morel (1991), Colimitation of phytoplankton growth by nickel and nitrogen, *Limnology and Oceanography*, *36*(6), 1071-1077.
Proshutinsky, A., R. Krishfield, M. L. Timmermans, J. Toole, E. Carmack, F. McLaughlin, W. J. Williams, S. Zimmermann, M. Itoh, and K. Shimada (2009), Beaufort Gyre freshwater reservoir: State and variability from observations, *Journal of Geophysical Research: Oceans*, *114*(C1).
Richon, C., and A. Tagliabue (2019), Insights Into the Major Processes Driving the Global Distribution of Copper in the Ocean From a Global Model, *Global Biogeochemical Cycles*, *33*(12), 1594-1610.
Rijkenberg, M. J. A., H. A. Slagter, M. Rutgers van der Loeff, J. van Ooijen, and L. J. A. Gerringa (2018), Dissolved Fe in the Deep and Upper Arctic Ocean With a Focus on Fe Limitation in the Nansen Basin, *Frontiers in Marine Science*, *5*(88).

Rudels, B. (2015), Arctic Ocean circulation, processes and water masses: A description of observations and ideas with focus on the period prior to the International Polar Year 2007–2009, *Progress in Oceanography*, *132*, 22-67.
Rudels, B., E. P. Jones, U. Schauer, and P. Eriksson (2004), Atlantic sources of the Arctic Ocean surface and halocline waters, *Polar Research*, *23*(2), 181-208.
Rysgaard, S., R. Glud, M. Sejr, J. Bendtsen, and P. Christensen (2007), Inorganic carbon transport during sea ice growth and decay: A carbon pump in polar seas, *Journal of Geophysical Research: Oceans*, *112*(C3).
Saito, M. A., J. W. Moffett, and G. R. DiTullio (2004), Cobalt and nickel in the Peru upwelling region: A major flux of labile cobalt utilized as a micronutrient, *Global Biogeochemical Cycles*, *18*(4).
Sakshaug, E. (2004), Primary and secondary production in the Arctic Seas, in *The organic carbon cycle in the Arctic Ocean*, edited, pp. 57-81, Springer.
Schauer, U., B. Rudels, E. Jones, L. Anderson, R. Muench, G. Björk, J. Swift, V. Ivanov, and A.-M. Larsson (2002), Confluence and redistribution of Atlantic water in the Nansen, Amundsen and Makarov basins, paper presented at Annales Geophysicae.
Schlitzer, R., et al. (2018), The GEOTRACES Intermediate Data Product 2017, *Chemical Geology*, *493*, 210-223.
Schlosser, P., B. Kromer, G. Östlund, B. Ekwurzel, G. Bönisch, H. Loosli, and R. Purtschert (1994), On the 14 C and 39 Ar Distribution in the Central Arctic Ocean: Implications for Deep Water Formation 1, *Radiocarbon*, *36*(3), 327-343.
Sclater, F., E. Boyle, and J. Edmond (1976), On the marine geochemistry of nickel, *Earth and Planetary Science Letters*, *31*(1), 119-128.
Sherrell, R. M., and E. A. Boyle (1992), The trace metal composition of suspended particles in the oceanic water column near Bermuda, *Earth and Planetary Science Letters*, *111*(1), 155-174.
Shimada, K., M. Itoh, S. Nishino, F. McLaughlin, E. Carmack, and A. Proshutinsky (2005), Halocline structure in the Canada Basin of the Arctic Ocean, *Geophysical Research Letters*, *32*(3), n/a-n/a.
Slagter, H. A., L. M. Laglera, C. Sukekava, and L. J. A. Gerringa (2019), Fe-Binding Organic Ligands in the Humic-Rich TransPolar Drift in the Surface Arctic Ocean Using Multiple Voltammetric Methods, *Journal of Geophysical Research: Oceans*, *124*(3), 1491-1508.
Slagter, H. A., H. E. Reader, M. J. A. Rijkenberg, M. Rutgers van der Loeff, H. J. W. de Baar, and L. J. A. Gerringa (2017), Organic Fe speciation in the Eurasian Basins of the Arctic Ocean and its relation to terrestrial DOM, *Marine Chemistry*, *197*, 11-25.
Spivack, A. J., S. S. Huested, and E. A. Boyle (1983), Copper, Nickel and Cadmium in the Surface Waters of the Mediterranean, in *Trace Metals in Sea Water*, edited by C. S. Wong, E. Boyle, K. W. Bruland, J. D. Burton and E. D. Goldberg, pp. 505-512, Springer US, Boston, MA.
Steele, M., J. Morison, W. Ermold, I. Rigor, M. Ortmeyer, and K. Shimada (2004), Circulation of summer Pacific halocline water in the Arctic Ocean, *Journal of Geophysical Research: Oceans*, *109*(C2).
Sunda, W. G. (2012), Feedback interactions between trace metal nutrients and phytoplankton in the ocean, *Frontiers in Microbiology*, *3*.
Talley, L. D., G. L. Pickard, W. J. Emery, and J. H. Swift (2011), Chapter 12 - Arctic Ocean and Nordic Seas, in *Descriptive Physical Oceanography (Sixth Edition)*, edited, pp. 401-436, Academic Press, Boston.

Tanhua, T., E. P. Jones, E. Jeansson, S. Jutterström, W. M. Smethie, D. W. R. Wallace, and L. G. Anderson (2009), Ventilation of the Arctic Ocean: Mean ages and inventories of anthropogenic CO2 and CFC-11, *Journal of Geophysical Research: Oceans*, *114*(C1), n/a-n/a.
Taylor, R. L., D. M. Semeniuk, C. D. Payne, J. Zhou, J. É. Tremblay, J. T. Cullen, and M. T. Maldonado (2013), Colimitation by light, nitrate, and iron in the Beaufort Sea in late summer, *Journal of Geophysical Research: Oceans*, *118*(7), 3260-3277.
Timmermans, M.-L., C. Garrett, and E. Carmack (2003), The thermohaline structure and evolution of the deep waters in the Canada Basin, Arctic Ocean, *Deep Sea Research Part I: Oceanographic Research Papers*, *50*(10), 1305-1321.
Tovar-Sánchez, A., C. M. Duarte, J. C. Alonso, S. Lacorte, R. Tauler, and C. Galbán-Malagón (2010), Impacts of metals and nutrients released from melting multiyear Arctic sea ice, *Journal of Geophysical Research: Oceans*, *115*(C7), n/a-n/a.
Twining, B. S., and S. B. Baines (2013), The trace metal composition of marine phytoplankton, *Annual review of marine science*, *5*, 191-215.
Twining, B. S., S. B. Baines, S. Vogt, and D. M. Nelson (2012), Role of diatoms in nickel biogeochemistry in the ocean, *Global biogeochemical cycles*, *26*(4).
Vieira, L. H., E. P. Achterberg, J. Scholten, A. J. Beck, V. Liebetrau, M. M. Mills, and K. R. Arrigo (2019), Benthic fluxes of trace metals in the Chukchi Sea and their transport into the Arctic Ocean, *Marine Chemistry*, *208*, 43-55.
Vraspir, J. M., and A. Butler (2009), Chemistry of marine ligands and siderophores.
Westerlund, S. F. G., L. G. Anderson, P. O. J. Hall, Å. Iverfeldt, M. M. R. Van Der Loeff, and B. Sundby (1986), Benthic fluxes of cadmium, copper, nickel, zinc and lead in the coastal environment, *Geochimica et Cosmochimica Acta*, *50*(6), 1289-1296.
Whitby, H., and C. M. van den Berg (2015), Evidence for copper-binding humic substances in seawater, *Marine Chemistry*, *173*, 282-290.
Wood, P. M. (1978), Interchangeable Copper and Iron Proteins in Algal Photosynthesis: Studies on Plastocyanin and Cytochrome c-552 in Chlamydomonas, *European journal of biochemistry*, *87*(1), 9-19.
Woodgate, R. A., K. Aagaard, J. H. Swift, K. K. Falkner, and W. M. Smethie (2005), Pacific ventilation of the Arctic Ocean's lower halocline by upwelling and diapycnal mixing over the continental margin, *Geophysical Research Letters*, *32*(18), n/a-n/a.
Woodgate, R. A., K. Aagaard, R. D. Muench, J. Gunn, G. Björk, B. Rudels, A. T. Roach, and U. Schauer (2001), The Arctic Ocean Boundary Current along the Eurasian slope and the adjacent Lomonosov Ridge: Water mass properties, transports and transformations from moored instruments, *Deep Sea Research Part I: Oceanographic Research Papers*, *48*(8), 1757-1792.
Xiang, Y., and P. J. Lam (2020), Size-fractionated compositions of marine suspended particles in the Western Arctic Ocean: lateral and vertical sources, *Journal of Geophysical Research: Oceans*, *n/a*(n/a), e2020JC016144.
Yamamoto-Kawai, M., F. McLaughlin, E. Carmack, S. Nishino, and K. Shimada (2008), Freshwater budget of the Canada Basin, Arctic Ocean, from salinity, δ18O, and nutrients, *Journal of Geophysical Research: Oceans*, *113*(C1).
Yamamoto-Kawai, M., F. McLaughlin, E. Carmack, S. Nishino, K. Shimada, and N. Kurita (2009), Surface freshening of the Canada Basin, 2003–2007: River runoff versus sea ice meltwater, *Journal of Geophysical Research: Oceans*, *114*(C1).
Yeats, P. A. (1988), Manganese, nickel, zinc and cadmium distributions at the Fram-3 and Cesar Ice Camps in the Arctic Ocean, *Oceanologica acta*, *11*(4), 383-388.

1109 Yeats, P. A., and S. Westerlund (1991), Trace metal distributions at an Arctic Ocean ice island,
1110 *Marine Chemistry*, *33*(3), 261-277.
1111 Yeats, P. A., S. Westerlund, and A. R. Flegal (1995), Cadmium, copper and nickel distributions
1112 at four stations in the eastern central and south Atlantic, *Marine Chemistry*, *49*(4), 283-293.
1113 Zhang, R., L. T. Jensen, J. N. Fitzsimmons, R. M. Sherrell, and S. John (2019), Dissolved
1114 cadmium and cadmium stable isotopes in the western Arctic Ocean, *Geochimica et*
1115 *Cosmochimica Acta*, *258*, 258-273.
1116

CRM		GN01 Element (nmol/kg)			GN02/03* Element (nmol/kg)			GN04** Element (nmol/kg)		Consensus value Element (nmol/kg)	
	n	Ni	Cu	n	Ni	Cu	n	Ni	Cu	Ni	Cu
SAFe D1	35	8.609	2.035	14	8.64	2.15	6	8.54	1.990	8.580	2.270
stdev		0.176	0.081		0.30	0.09		0.084	0.020	0.260	0.110
SAFe D2	32	8.714	2.192							8.630	2.280
stdev		0.166	0.099							0.250	0.150
SAFe S	4	2.401	0.544	14	2.31	0.49				2.280	0.520
stdev		0.020	0.013		0.09	0.05				0.090	0.050
		Element (pmol/kg)			Element (pmol/kg)			Element (pmol/kg)			
	n	Ni	Cu	n	Ni	Cu	n	Ni	Cu		
Average blank	31	15.2	12.4	10	53	30	24	7.4	8.2		
Std deviation of blank	29	2.82	1.69	10	10	2.7	24	4.00	10.70		
Detection limit (3*stdev)	29	8.45	5.08	10	30	8	24	12.00	32.10		

	Cu (nmol/kg)	Ni (nmol/kg)
GN01 (0-20m)	4.57 ± 1.50	6.59 ± 1.25
GN02 (0-20m)	3.17 ± 0.65	4.93 ± 0.83
GN03 (0-20m)	3.98 ± 0.31	6.37 ± 0.70
GN04 (0-20m)	3.64 ± 2.09	5.20 ± 2.02
Global (0-20m)	0.80 ± 0.64	3.18 ± 1.53
Cu/Ni relationship (0-20m)	dCu = [0.95(±0.03)]*dNi – 1.53(±0.18), r^2 = 0.88	
Cu/Ni relationship pan-Arctic all depths	dCu = [0.841(±0.01)]*dNi – 1.35(±0.05), r^2 = 0.87	

	Cu (nmol/kg)	Ni (nmol/kg)
Canada Basin (>1800m)	1.42 ± 0.11	3.09 ± 0.09
Makarov Basin (>1800m)	1.40 ± 0.11	3.15 ± 0.07
Amundsen Basin (>1800m)	1.56 ± 0.07	3.53 ± 0.08
Nansen Basin (>1800m)	1.59 ± 0.05	3.61 ± 0.10
All basins (>1800m)	1.57 ± 0.47	3.40 ± 0.35
Global average (>1000m)	2.60 ± 1.02	7.76 ± 1.56

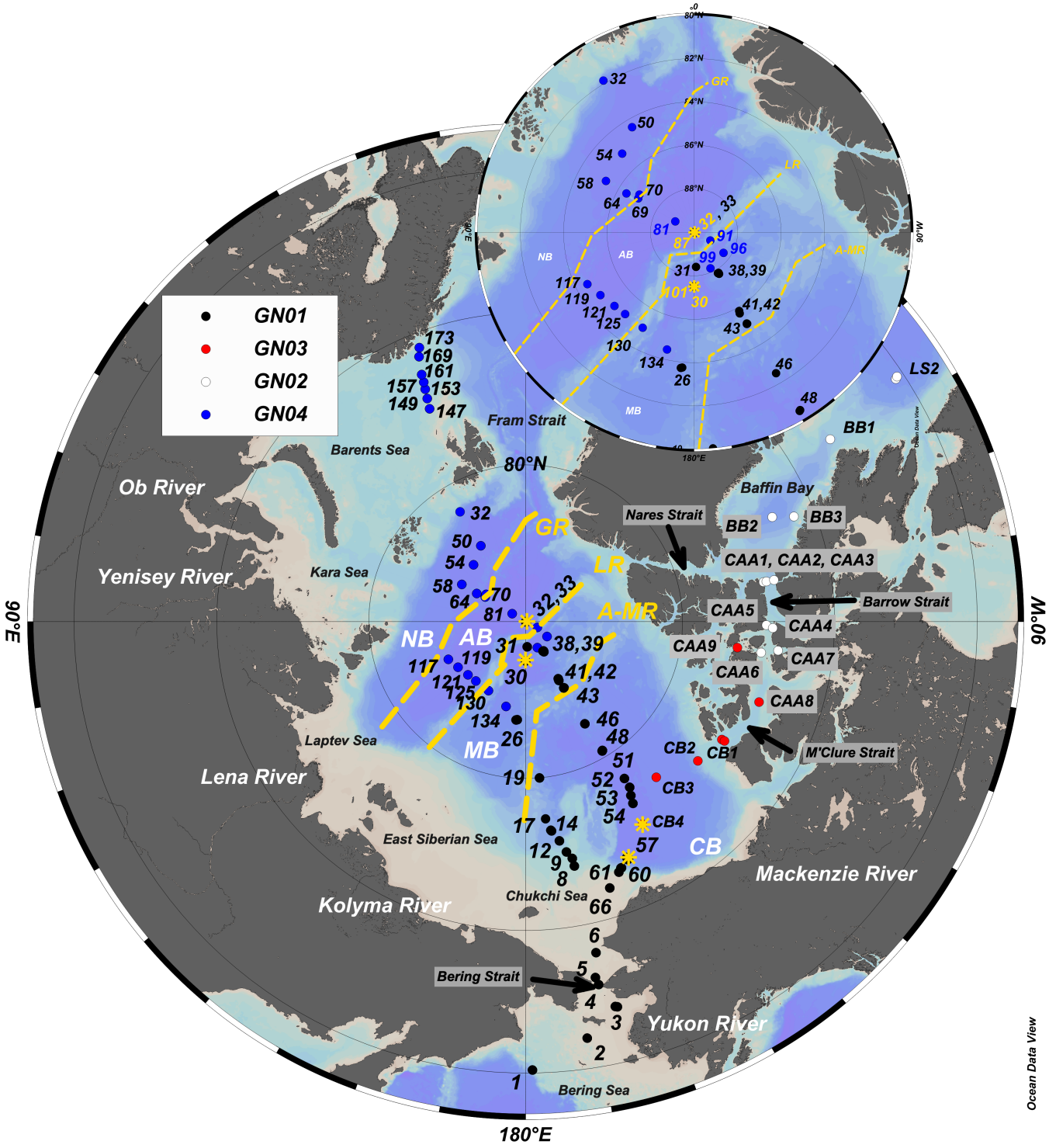
GN01
GN03
GN02
GN04
Fram Strait
Barents Sea
Ob River
Yenisey River
Kara Sea
Laptev Sea
Lena River
East Siberian Sea
Kolyma River
Chukchi Sea
Bering Strait
Bering Sea
Yukon River
Mackenzie River
Baffin Bay
Nares Strait
Barrow Strait
M'Clure Strait
LS2
BB1
BB2
BB3
CAA1, CAA2, CAA3
CAA4
CAA5
CAA6
CAA7
CAA8
CAA9
CB1
CB2
CB3
CB4
CB
GR
LR
A-MR
NB
AB
MB
80°N
90°E
90°W
180°E
Ocean Data View

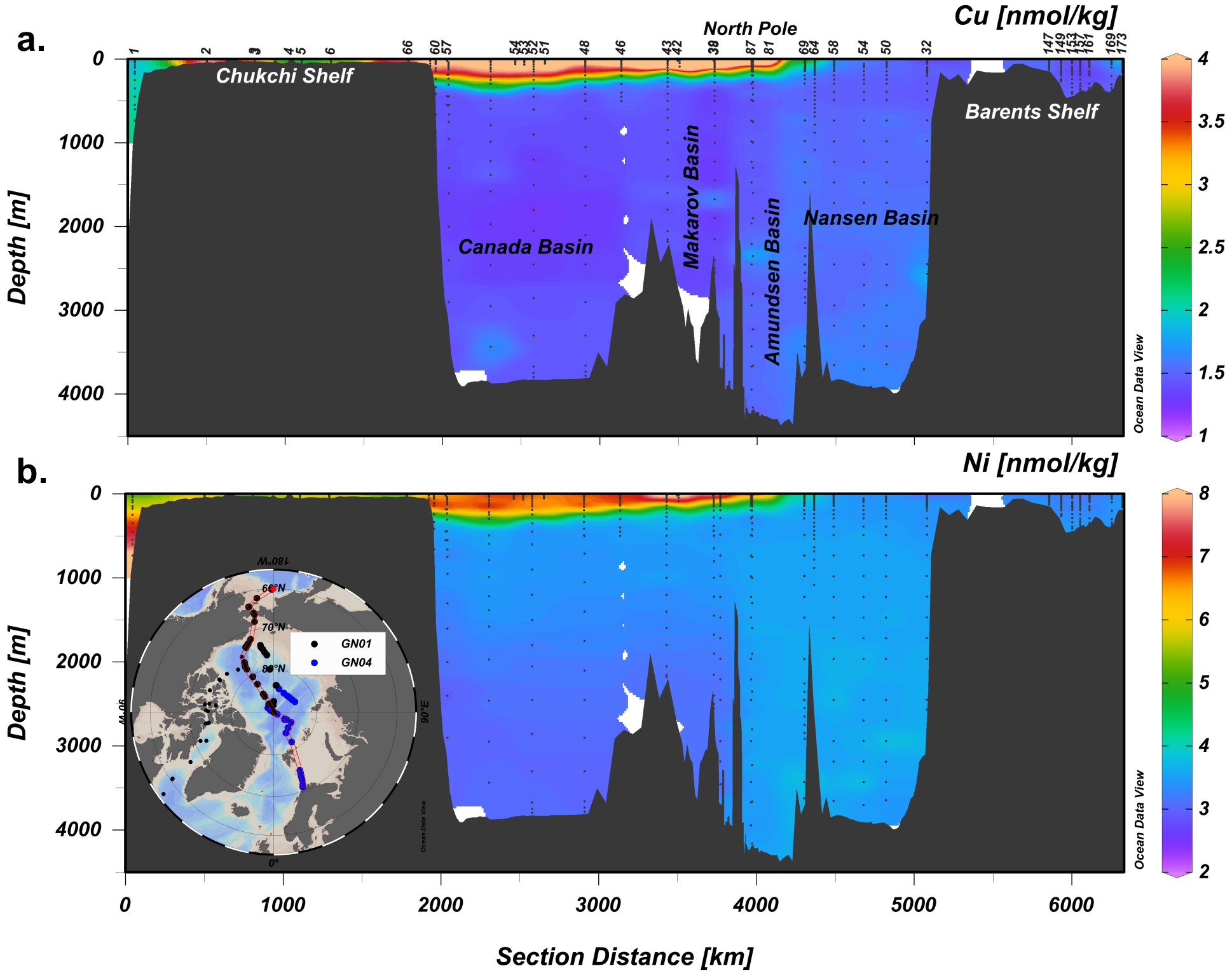
a.
Cu [nmol/kg]
North Pole
Chukchi Shelf
Canada Basin
Makarov Basin
Amundsen Basin
Nansen Basin
Barents Shelf
Depth [m]
0
1000
2000
3000
4000
Ocean Data View
4
3.5
3
2.5
2
1.5
1
b.
Ni [nmol/kg]
GN01
GN04
60°N
70°N
80°N
90°E
0°
8
7
6
5
4
3
2
0
1000
2000
3000
4000
5000
6000
Section Distance [km]

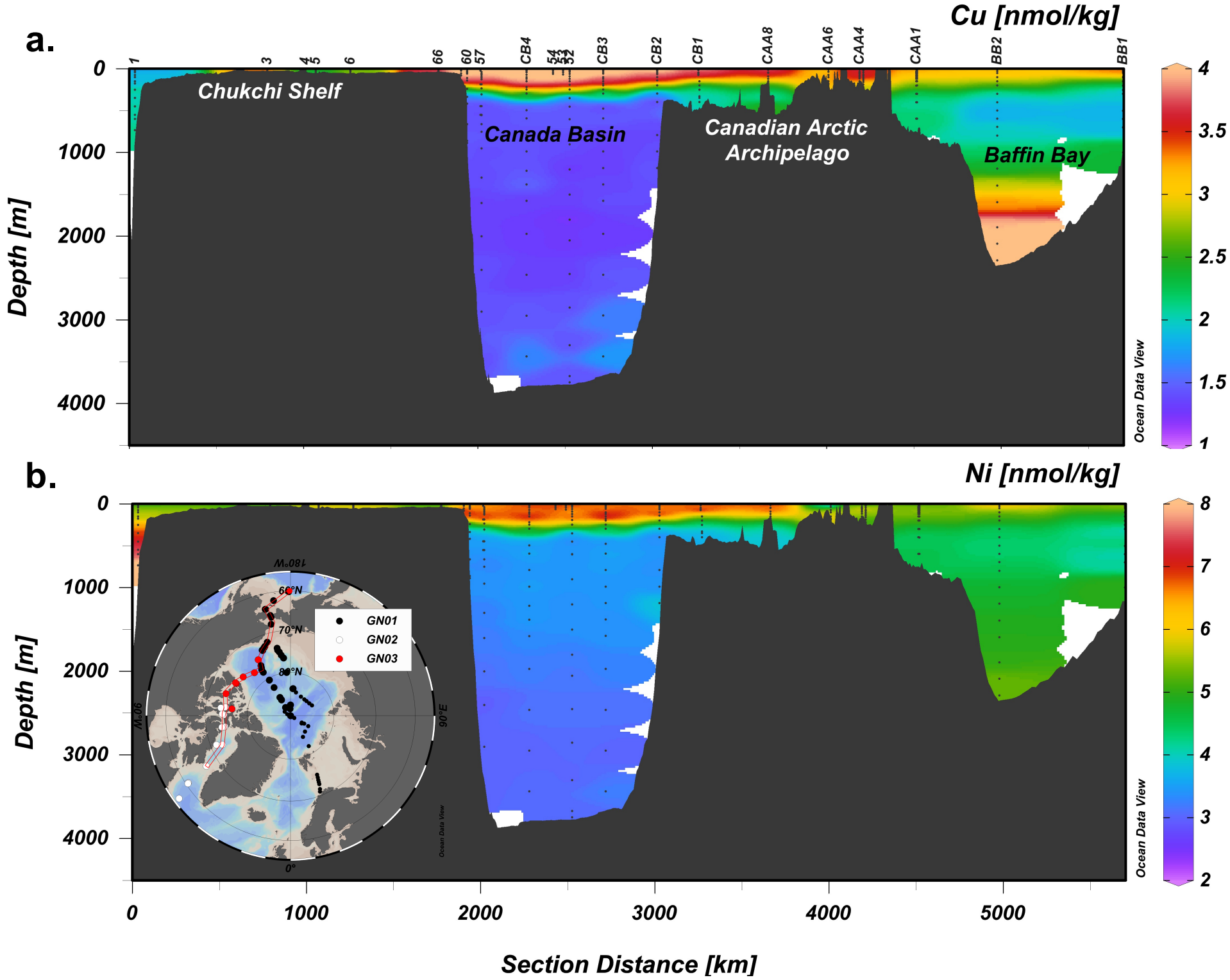
a.
Cu [nmol/kg]
Chukchi Shelf
Canada Basin
Canadian Arctic Archipelago
Baffin Bay
1
3
4
5
6
66
60
57
CB4
54
53
52
CB3
CB2
CB1
CAA8
CAA6
CAA4
CAA1
BB2
BB1
Depth [m]
0
1000
2000
3000
4000
4
3.5
3
2.5
2
1.5
1
Ocean Data View
b.
Ni [nmol/kg]
GN01
GN02
GN03
66°N
70°N
80°N
180°W
90°W
0°
90°E
0
1000
2000
3000
4000
5000
8
7
6
5
4
3
2
Section Distance [km]

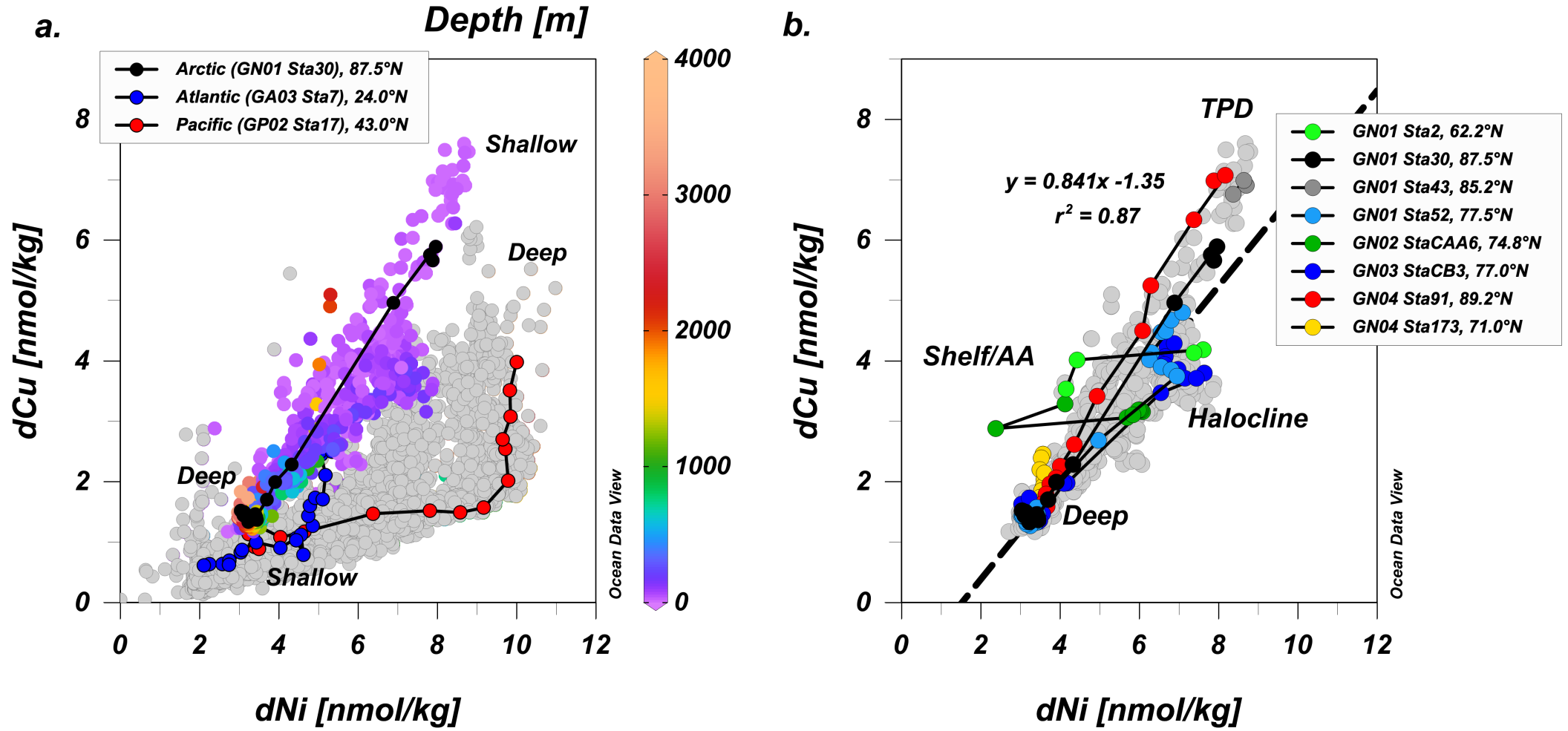
a.
Depth [m]
Arctic (GN01 Sta30), 87.5°N
Atlantic (GA03 Sta7), 24.0°N
Pacific (GP02 Sta17), 43.0°N
Shallow
Deep
Deep
Shallow
4000
3000
2000
1000
0
Ocean Data View
dCu [nmol/kg]
dNi [nmol/kg]
0
2
4
6
8
10
12
b.
TPD
y = 0.841x -1.35
r2 = 0.87
Shelf/AA
Halocline
Deep
GN01 Sta2, 62.2°N
GN01 Sta30, 87.5°N
GN01 Sta43, 85.2°N
GN01 Sta52, 77.5°N
GN02 StaCAA6, 74.8°N
GN03 StaCB3, 77.0°N
GN04 Sta91, 89.2°N
GN04 Sta173, 71.0°N
Ocean Data View
dCu [nmol/kg]
dNi [nmol/kg]

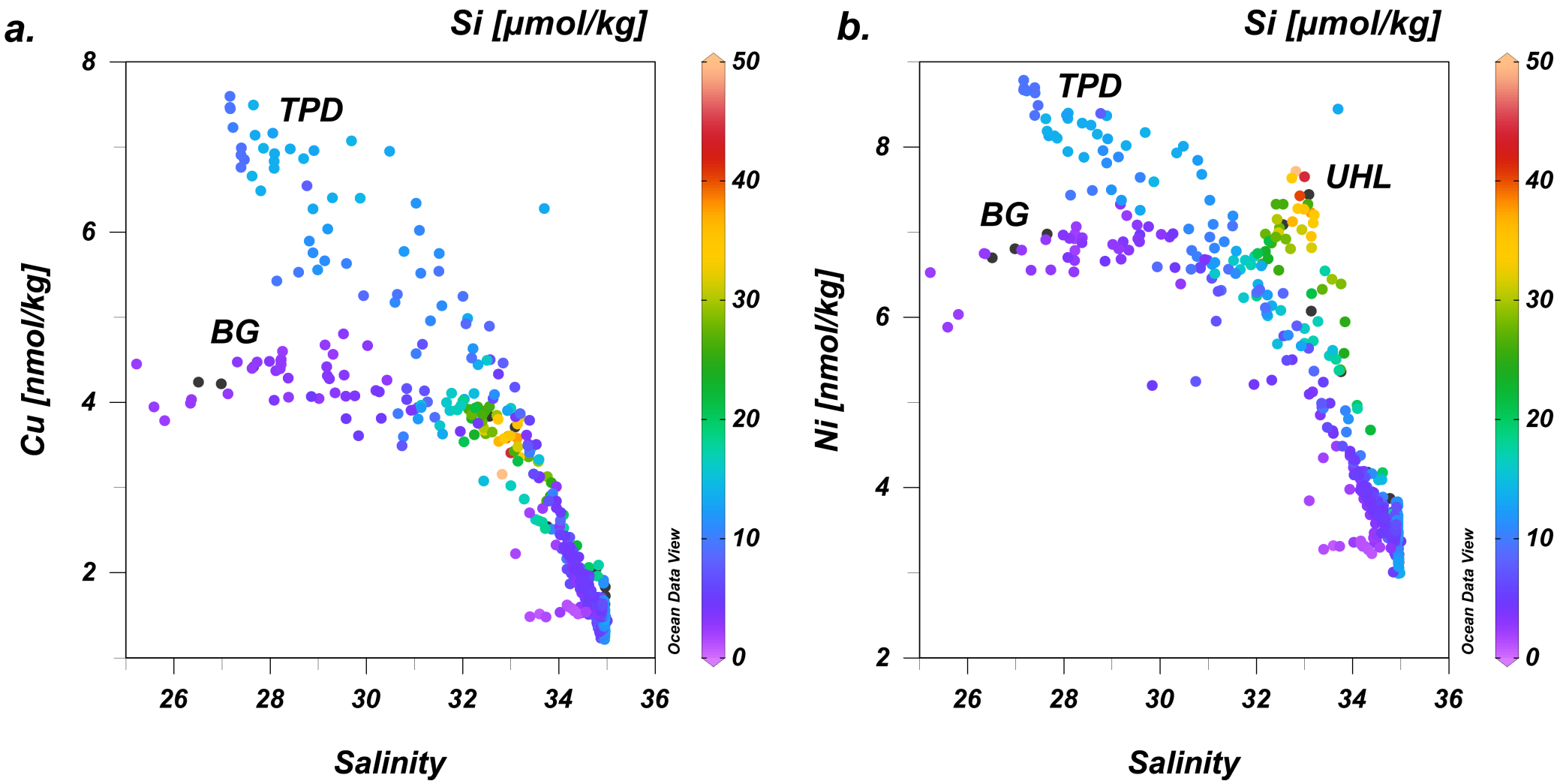
a.
Si [µmol/kg]
TPD
BG
Cu [nmol/kg]
Salinity
Ocean Data View
b.
Si [µmol/kg]
TPD
UHL
BG
Ni [nmol/kg]
Salinity
Ocean Data View

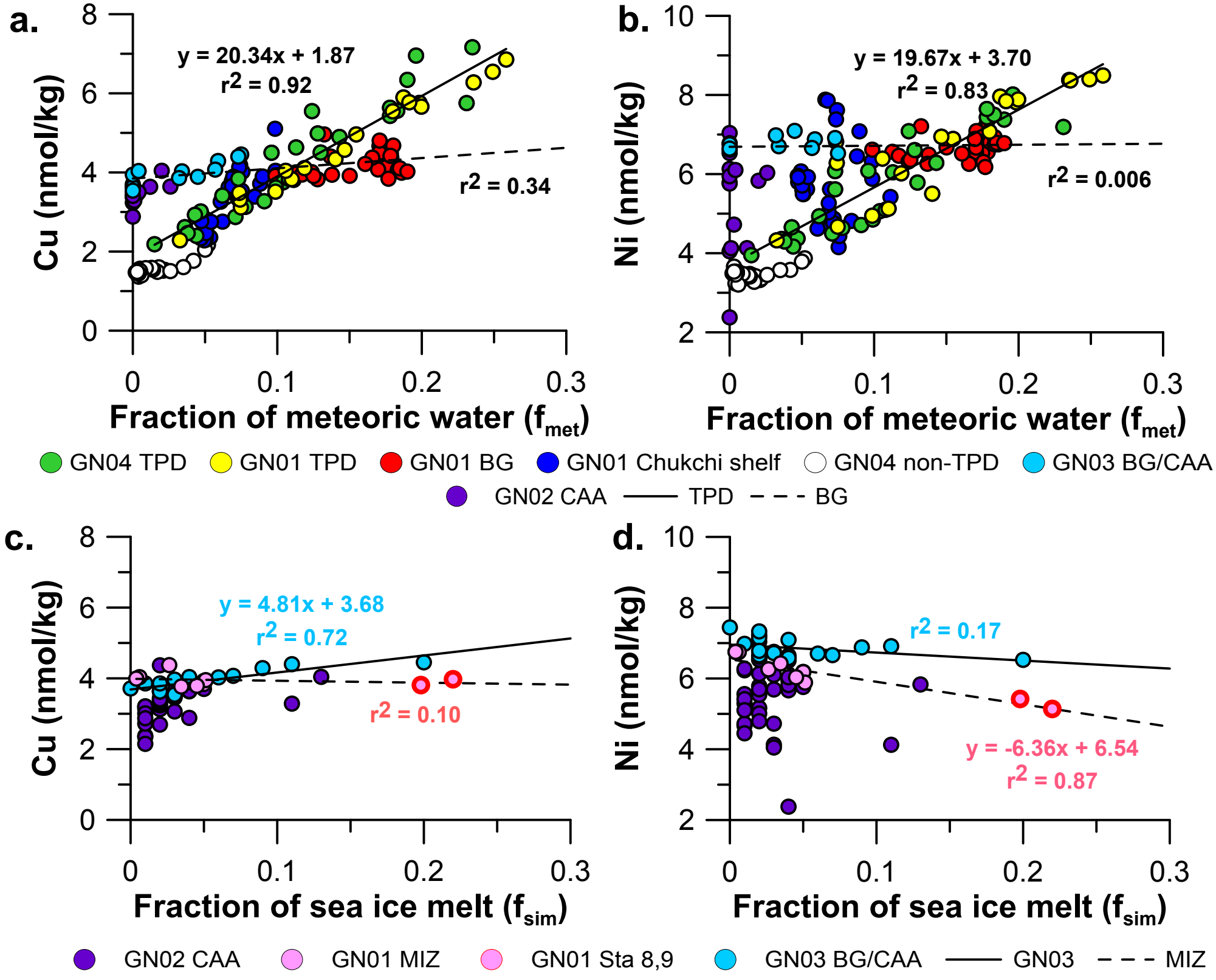
a.
y = 20.34x + 1.87
r2 = 0.92
r2 = 0.34
Cu (nmol/kg)
Fraction of meteoric water (fmet)
b.
y = 19.67x + 3.70
r2 = 0.83
r2 = 0.006
Ni (nmol/kg)
Fraction of meteoric water (fmet)
GN04 TPD
GN01 TPD
GN01 BG
GN01 Chukchi shelf
GN04 non-TPD
GN03 BG/CAA
GN02 CAA
TPD
BG
c.
y = 4.81x + 3.68
r2 = 0.72
r2 = 0.10
Cu (nmol/kg)
Fraction of sea ice melt (fsim)
d.
r2 = 0.17
y = -6.36x + 6.54
r2 = 0.87
Ni (nmol/kg)
Fraction of sea ice melt (fsim)
GN02 CAA
GN01 MIZ
GN01 Sta 8,9
GN03 BG/CAA
GN03
MIZ

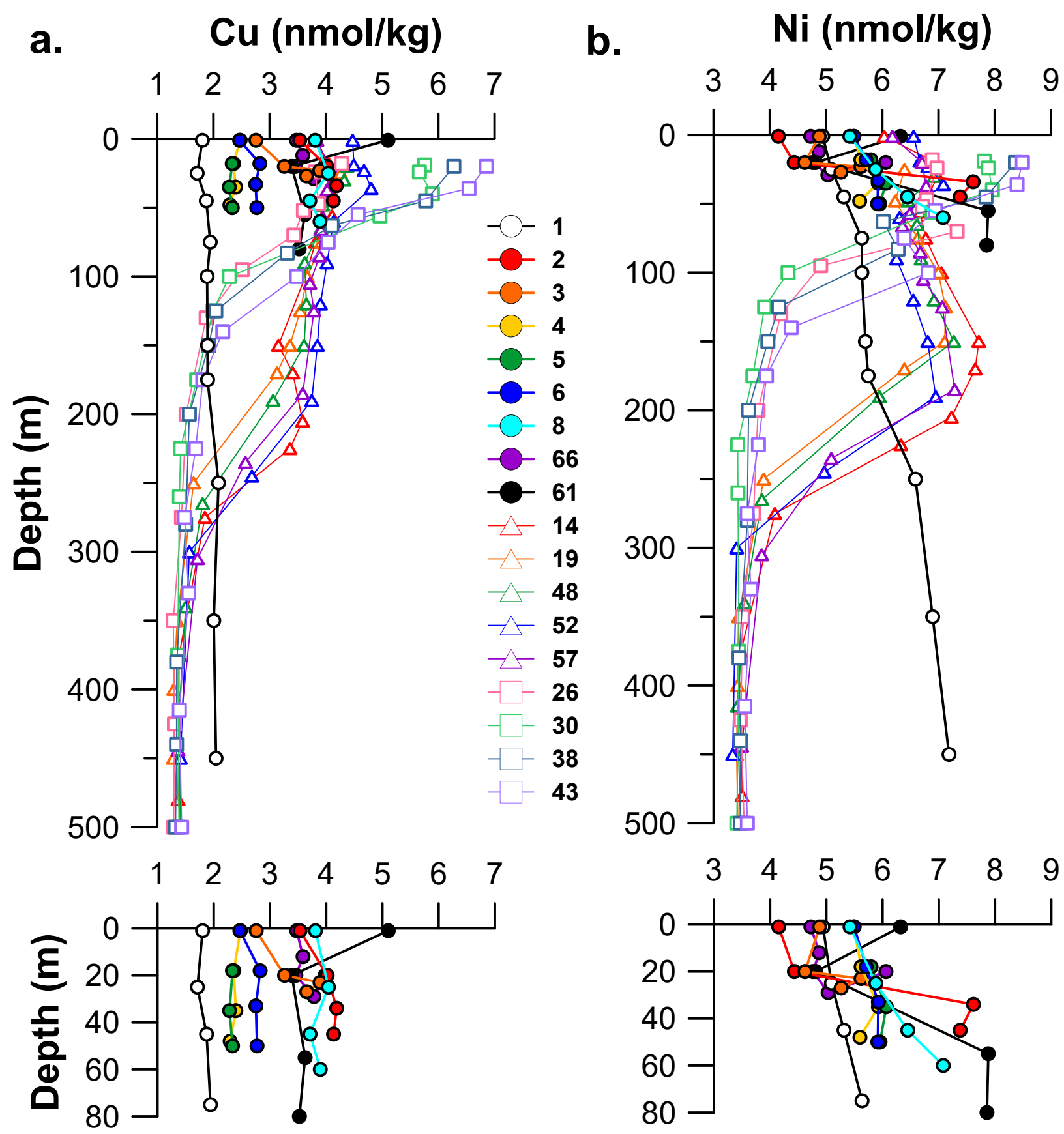
a.
Cu (nmol/kg)
b.
Ni (nmol/kg)
Depth (m)
1
2
3
4
5
6
8
66
61
14
19
48
52
57
26
30
38
43

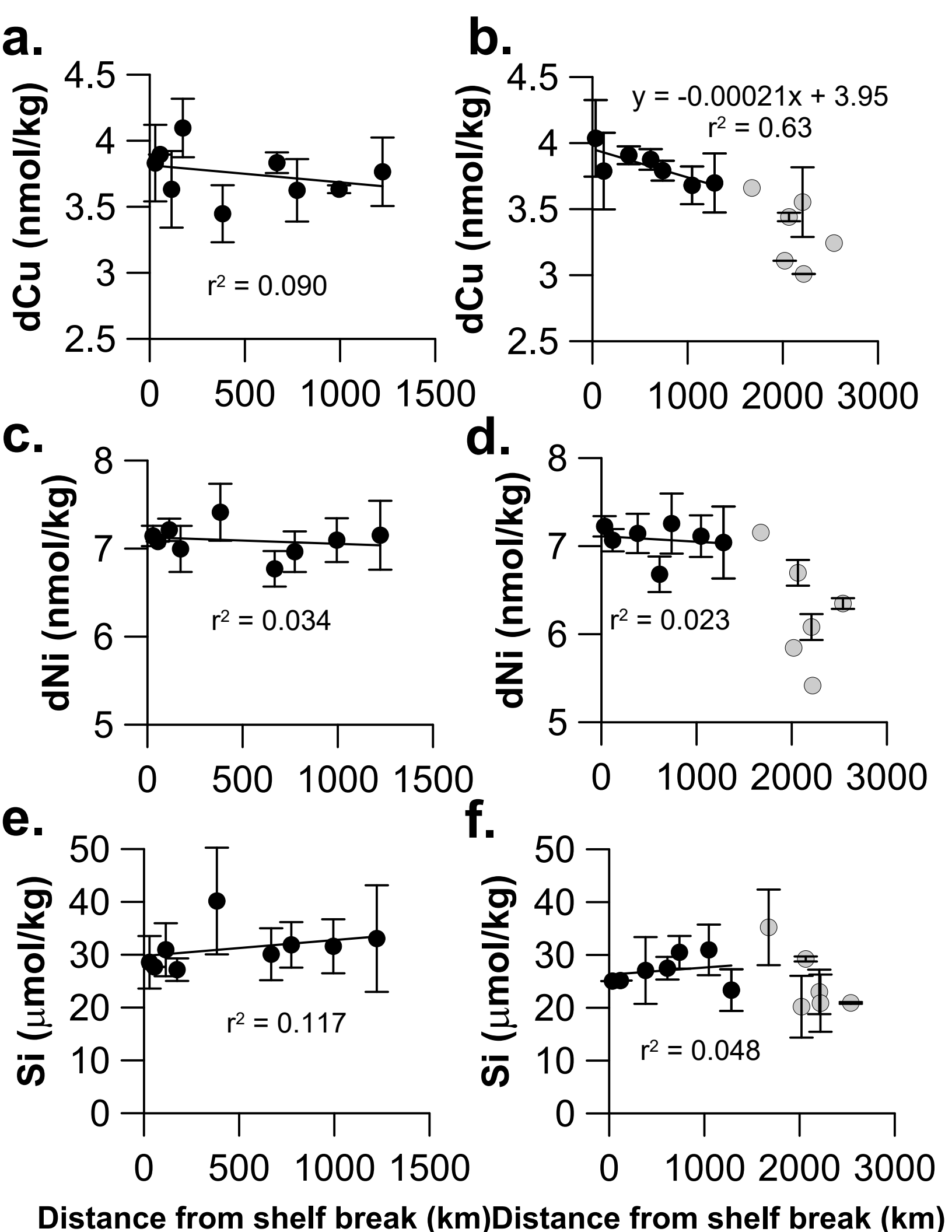
a.
b.
c.
d.
e.
f.
dCu (nmol/kg)
dNi (nmol/kg)
Si (μmol/kg)
y = -0.00021x + 3.95
r² = 0.63
r² = 0.090
r² = 0.034
r² = 0.023
r² = 0.117
r² = 0.048
Distance from shelf break (km)
Distance from shelf break (km)

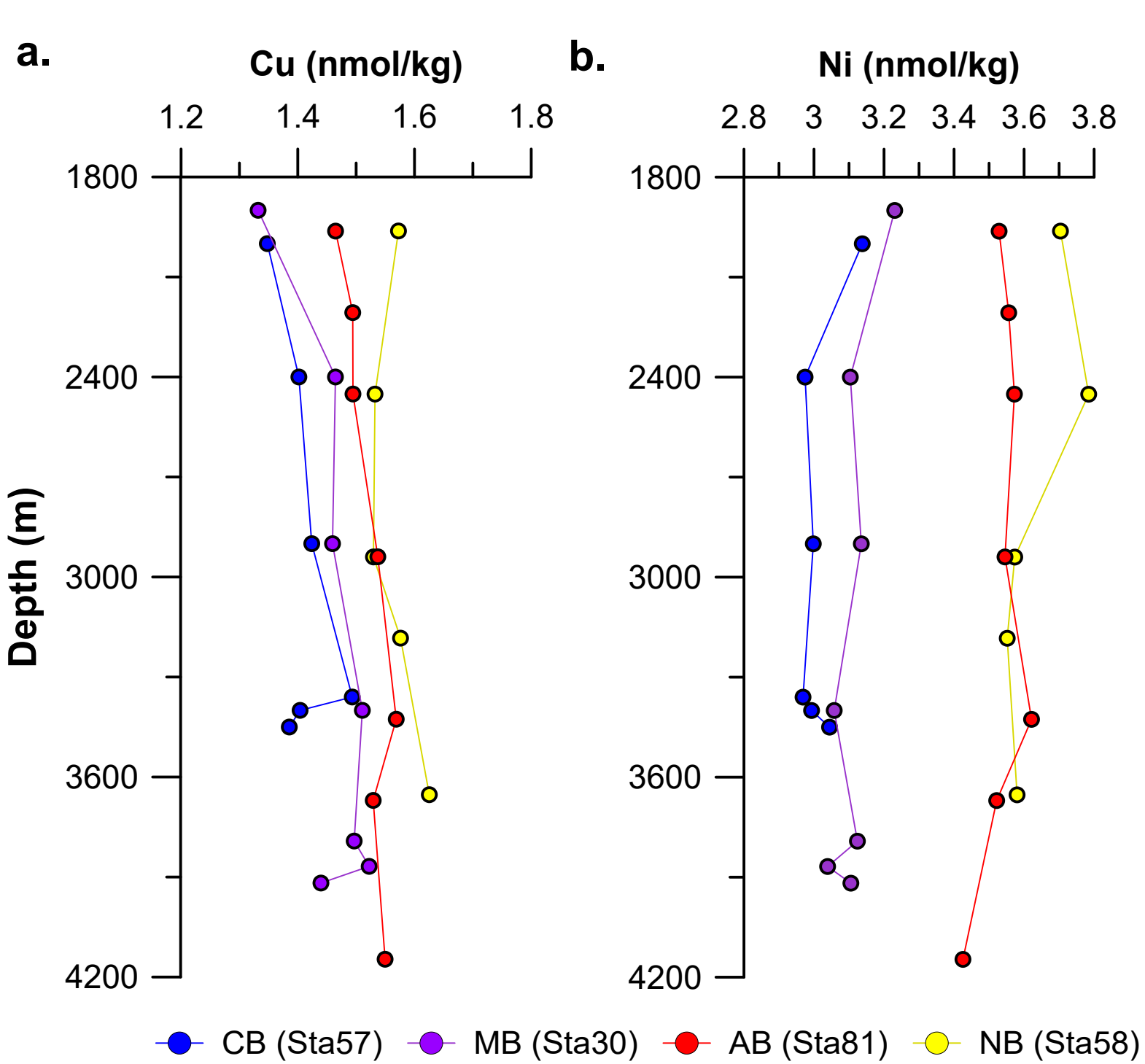
a.
Cu (nmol/kg)
1.2
1.4
1.6
1.8
b.
Ni (nmol/kg)
2.8
3
3.2
3.4
3.6
3.8
Depth (m)
1800
2400
3000
3600
4200
CB (Sta57)
MB (Sta30)
AB (Sta81)
NB (Sta58)